Mitochondrial permeabilisation engages NF-κB dependent anti-tumour activity under caspase deficiency

Evangelos Giampazolias [1,2], Barbara Zunino [1*], Sandeep Dhayade [1*], Florian Bock [1,2], Catherine Cloix [1,2], Kai Cao [1,2], Alba Roca [1,2], Jonathan Lopez [1,2,^], Gabriel Ichim [1,2,-^], Emma Proïcs [3], Camila Rubio-Patiño [3], Loic Fort [1], Nader Yatim [4], Emma Woodham [1], Susana Orozco [5], Lucia Taraborrelli [6], Nieves Peltzer [6], Daniele Lecis [7], Laura Machesky [1], Henning Walczak [6], Matthew L. Albert [4,8], Simon Milling [9], Andrew Oberst [5], Jean-Ehrland Ricci [3], Kevin M. Ryan [1], Karen Blyth [1], Stephen W.G. Tait [1,2*]

[1] Cancer Research UK Beatson Institute, [2] Institute of Cancer Sciences, University of Glasgow, Garscube Estate, Switchback Road, Glasgow, G61 1BD, U.K. [3] Université Côte d'Azur, Inserm, C3M, France. [4] Laboratory of Dendritic Cell Biology, Department of Immunology, Institut Pasteur, 25 Rue du Docteur Roux, 75015 Paris, France. [5] Molecular & Cellular Biology Program and Dept. of Immunology, University of Washington, 750 Republican St., Seattle, WA 981, U.S.A. [6] Centre for Cell Death, Cancer and Inflammation, UCL Cancer Institute, UCL, London WC1E 6BT, UK. [7] Department of Experimental Oncology and Molecular Medicine, Fondazione IRCCS Istituto Nazionale dei Tumori, Milan 20133, Italy. [8] Department of Cancer Immunology, Genentech Inc., 1 DNA way, South San Francisco, California 94080, USA [9] Centre for Immunobiology, Institute for Infection, Immunity and Inflammation, College of Medical, Veterinary and Life Sciences, University of Glasgow, Glasgow, U.K. . ^ Present address: University of Lyon, Cancer Research Centre of Lyon (CRCL), UMR INSERM 1052 CNRS 5286, Léon Bérard Centre, 28, Rue Laennec, 69008, Lyon, France. *These authors contributed equally.

*Correspondence should be addressed to (S.W.G.T): stephen.tait@glasgow.ac.uk

Running title: Anti-tumourigenic effects of caspase-independent cell death

Abstract

Apoptosis represents a key anti-cancer therapeutic effector mechanism. During apoptosis, mitochondrial outer membrane permeabilisation (MOMP) typically kills cells even in the absence of caspase activity. Caspase activity can also have a variety of unwanted consequences that include DNA-damage. We therefore investigated whether MOMP-induced caspase-independent cell death (CICD) might be a better way to kill cancer cells. We find that cells undergoing CICD display potent pro-inflammatory effects relative to apoptosis. Underlying this, MOMP was found to stimulate NF-κB activity through the down-regulation of inhibitor of apoptosis (IAP) proteins. Strikingly, engagement of CICD displays potent anti-tumorigenic effects, often promoting complete tumour regression in a manner dependent on intact immunity. Our data demonstrate that by activating NF-κB, MOMP can exert additional signalling functions besides triggering cell death. Moreover, they support a rationale for engaging caspase-independent cell death in cell-killing anti-cancer therapies.

Introduction

Mitochondrial outer membrane permeabilisation or MOMP, is often essential for apoptosis; MOMP enables the release of mitochondrial proteins, including cytochrome *c*, that activate caspases leading to rapid cell death [1]. Nevertheless, cells typically die following MOMP even in the absence of caspase activity, through a process called caspase-independent cell death (CICD). This defines MOMP as a point-of-no-return that commits a cell to die [2].

Apoptosis is broadly considered a positive process that can serve to both prevent and treat cancer [3]. However, various data argue that apoptosis may also have detrimental effects that are potentially tumour promoting [4, 5]. For instance, sub-lethal apoptotic stress can engage caspase activity in the absence of cell death, leading to DNA damage and genomic instability [6-8]. We have previously found that these effects were dependent upon MOMP in a limited cohort of mitochondria, permitting sub-lethal caspase activity [6].

Caspases are not required for MOMP-induced killing; this finding, coupled to the negative effects of engaging sub-lethal caspase activity, led us to ask whether CICD might be a better way to kill cancer cells. We find that under caspase-deficient conditions, MOMP can trigger TNF-dependent necroptosis as a form of CICD. Underlying this, MOMP triggers NF-κB activation during CICD, leading to pro-inflammatory and immunogenic effects. Most importantly, therapeutic engagement of CICD displays significantly enhanced anti-tumour activity relative to apoptosis.

Results

Mitochondrial permeabilisation can engage necroptosis as a form of caspase-independent cell death

Mitochondria are not required to execute necroptosis; however whether they can initiate this type of cell death is unclear [9]. We investigated whether mitochondrial permeabilisation could trigger necroptosis as a type of caspase-independent cell death (CICD). To induce apoptosis, SVEC cells were treated with the

BH3-mimetic ABT-737 +/- the pan-caspase inhibitor Q-VD-OPh. Caspase activity was determined by Western blotting for PARP1 cleavage and cell viability was measured by propidium iodide (PI) exclusion. ABT-737 treatment led to PARP1 cleavage that was blocked by Q-VD-OPh treatment (Figure 1A). ABT-737 triggered cell death irrespective of caspase-inhibition (Figure 1B) but in a MOMP-dependent manner, since MCL-1 expression (which is not effectively inhibited by ABT-737) prevented cell death (Figure 1C, Supplemental Figures 1A, 1B, 1C) [10]. To investigate whether necroptosis could contribute to CICD, we inhibited RIPK1 and RIPK3 – two kinases often essential for necroptosis [11]. SVEC cells were treated with ABT-737 +/- Q-VD-OPh together with necrostatin-1 (nec-1), to inhibit RIPK1, or following RIPK3 shRNA-knockdown (Supplemental Figure 1D). RIPK3 knockdown prevented necroptosis induced by TNF/zVAD treatment, confirming functional inhibition (Figure 1D). Neither nec-1 treatment nor RIPK3 knockdown had any effect upon ABT-737 mediated apoptosis (Figure 1E). Nevertheless, inhibition of RIPK1 or RIPK3 reduced CICD following BH3-mimetic treatment, demonstrating that necroptosis can be engaged following mitochondrial permeabilisation (Figure 1E). We investigated this further using BCL-xL dependent SVEC cells generated using our mito-priming method [3]. SVEC cells expressing GFP-tBID 2A BCL-xL (BCL-xL dependent SVEC cells) were treated with ABT-737 +/- Q-VD-OPh. Alternatively, we used BCL-xL dependent SVEC cells in which mitochondrial-dependent caspase activity was inhibited by APAF-1 shRNA knockdown [3]. Cell viability was measured using SYTOX Green exclusion and Incucyte cell imaging. Verifying their BCL-xL survival dependency, ABT-737 treatment led to rapid cell death (Figure 1F) and with expected slower kinetics, in the presence of Q-VD-OPh or following APAF-1 knockdown (Figure 1F). Q-VD-OPh treatment completely prevented PARP1, caspase-3, -7 and BID cleavage confirming effective caspase inhibition (Figure 1G and Supplemental Figure 1E). Using these cells we investigated whether necroptosis could contribute to CICD. BCL-xL dependent SVEC cells were treated with ABT-737 together with Q-VD-OPh and necroptosis was inhibited by nec-1 treatment, RIPK3 knockdown or by CRISPR/Cas-9 mediated deletion of the essential necroptosis executioner protein MLKL (Figures 1H, 1I and 1J, Supplemental Figures 1F - H). In all cases, cell death was reduced following ABT-

737/Q-VD-OPh treatment. Therefore, mitochondrial permeabilisation can engage necroptosis as a form of caspase-independent cell death.

MOMP induces TNF synthesis under caspase-deficient conditions

We reasoned that MOMP might trigger necroptosis directly by activating RIPK1/RIPK3 or, indirectly, via TNF signalling. To discriminate these possibilities, SVEC cells were treated to undergo CICD in the presence of nec-1 (to inhibit RIPK1) or Enbrel (TNF-receptor-II/IgG fusion protein) to inhibit TNF signalling. Cell viability was measured by PI exclusion (Figure 2A). As before, ABT-737/Q-VD-OPh induced CICD in a nec-1 sensitive manner. Neither Enbrel nor nec-1 treatment impacted on ABT-737 mediated apoptosis (Figure 2A). However, inhibition of TNF signalling by Enbrel treatment reduced cell-death following ABT-737/Q-VD-OPh treatment that was not further inhibited by nec-1 treatment (Figure 2A). Similar results were obtained using BCL-xL-dependent-SVEC cells (Figure 2B). This demonstrates that MOMP-induced necroptosis requires TNF. In a reciprocal manner, exogenous TNF massively enhanced CICD following ABT-737 treatment that was inhibited by either RIPK3 knockdown or nec-1 treatment (Figure 2C). Therefore, under caspase-inhibited conditions, MOMP can engage and sensitise to TNF-dependent necroptosis. We asked whether MOMP could trigger TNF synthesis. BCL-xL dependent SVEC cells were treated with ABT-737 +/- Q-VD-OPh and analysed by qRT-PCR for *Tnf* mRNA transcript level (Figure 2D). Under caspase-inhibited conditions, ABT-737 treatment led to an increase in *Tnf* transcript level (Figure 2D) in a MOMP-dependent manner (Figure 2E, Supplemental Figure 1I). Using an ELISA, we also confirmed an increase in extracellular TNF protein level following engagement of CICD (Figure 2F). To extend these findings, we used cells in which mitochondrial-dependent caspase activity was inhibited by APAF-1 knockdown [3] or by CRISPR/Cas-9 deletion of caspase-9 (Supplemental Figure 1J). In both settings, ABT-737 treatment led to an increase in TNF transcript levels (Figures 2G, 2H). The MOMP-dependent increase of *Tnf* transcript was necroptosis independent since it was not impacted by MLKL deletion (Supplemental Figure 1K). Finally, we assayed *Tnf* transcript levels in BCL-xL-dependent-MEFs following ABT-737 treatment in the presence of Q-VD-OPh. Similar to SVEC cells, *Tnf* mRNA was also increased in MEFs following ABT-737 treatment,

dependent on caspase inhibition (Figure 2I).

Mitochondrial permeabilisation activates NF-κB

Given a major role of TNF in inflammation, we aimed to understand how MOMP could drive inflammatory signals in caspase-deficient settings, hypothesising that MOMP might activate NF-κB - a key pro-inflammatory transcriptional regulator. BCL-xL dependent SVEC cells were treated with ABT-737 and NF-κB activation was measured by NF-κB p65 nuclear translocation. Importantly, ABT-737 treatment led to NF-κB activation in a manner that was significantly increased under caspase-deficient conditions (Figures 3A and 3B). BAX/BAK deleted SVEC cells failed to activate NF-κB following ABT-737 treatment, demonstrating its MOMP dependence (Figures 3C, 3D, Supplemental Figure 2A). Inhibiting mitochondrial-dependent caspase activity by APAF-1 shRNA-knockdown or by caspase-9 CRISPR/Cas9 deletion also enabled NF-κB activation following ABT-737 treatment (Supplemental Figures 2B, 2C). Moreover, CRISPR/Cas9-mediated deletion of IKKβ or NEMO (also called IKK γ) inhibited NF-κB p65 nuclear translocation following ABT-737/Q-VD-OPh treatment (Supplemental Figures 2D, 2E). Consistent with an ability of MOMP to activate NF-κB, IκBα phosphorylation and degradation was detected following ABT-737 treatment in caspase-deficient settings. Loss of IκBα, but not phosphorylation was also observed in cells treated with ABT-737 to undergo apoptosis, in line with IκBα being a reported caspase substrate (Figure 3E)[12]. Using luciferase-based reporter constructs, ABT-737 treatment was also found to increase NF-κB transcriptional activity under caspase-inhibited conditions (Figure 3F). Combined ABT-737/Q-VD-OPh treatment also led to NF-κB activation in MEF and HeLa cells (Supplemental Figure 2F). Importantly, neither Enbrel treatment nor MLKL-deletion affected ABT-737/Q-VD-OPh induced NF-κB p65 translocation, demonstrating that MOMP-induced NF-κB activation is TNF and necroptosis independent (Supplemental Figures 2G and 2H). To investigate whether *Tnf* mRNA up-regulation following MOMP required NF-κB we expressed $I\kappa B^{SR}$ (super repressor) - a non-degradable IκBα that inhibits NF-κB nuclear translocation [13]. Inhibition of NF-κB activity by $I\kappa B^{SR}$ expression was verified

by inhibition of NF-κB p65 nuclear translocation following MOMP and increased cell death following TNF treatment (Figure 3G, Supplemental Figures 2I, 2J). Importantly, $I\kappa B^{SR}$ expression completely prevented *Tnf* mRNA up-regulation following ABT-737 treatment, confirming its NF-κB dependence (Figure 3H). $I\kappa B^{SR}$ expression also inhibited cell death following ABT-737/Q-VD-OPh treatment, consistent with a role for MOMP-dependent TNF synthesis in necroptosis engagement (Supplemental Figure 2K). These data demonstrate that under caspase-deficient conditions, MOMP potently activates NF-κB leading to the expression of pro-inflammatory TNF.

MOMP activates NF-κB through IAP down-regulation and NIK activation

We next sought to understand how mitochondrial permeabilisation could trigger NF-κB activity. Small molecules called SMAC-mimetics can activate NF-κB by causing IAP protein degradation leading to NIK stabilisation and activation [14, 15]. Because these molecules mimic the mitochondrial protein SMAC (also called DIABLO), which is released from mitochondria following MOMP – we hypothesised that MOMP might activate NF-κB through a similar mechanism (Supplemental Figure 3A). BCL-xL dependent SVEC cells were treated with ABT-737 together with Q-VD-OPh or with SMAC-mimetic (SM-83), and cell lysates were probed for c-IAP1, NIK and XIAP (Figure 4A). Supporting previous data, SMAC-mimetic (SM-83) treatment led to cIAP1 down-regulation and a concomitant increase of NIK (Figure 4A) [14, 15]. Phenocopying this effect, combined ABT-737/Q-VD-OPh treatment also triggered cIAP1 loss, NIK up-regulation and, additionally, XIAP depletion. cIAP1 and XIAP loss was partially inhibited by the proteasome inhibitor MG132, indicating that they were targeted for proteasomal degradation following MOMP (Supplemental Figure 3B). Similar effects were observed in MEF and HeLa cells following ABT-737 treatment (Supplemental Figure 3C). Demonstrating a MOMP dependency, combined ABT-737/Q-VD-OPh treatment triggered a loss of cIAP1, XIAP and an increase in NIK that was completely blocked in BAX/BAK deleted cells (Figure 4B). These data demonstrate that MOMP can signal IAP-protein degradation and NIK up-regulation. We investigated whether this was required for MOMP-dependent NF-κB activity by generating NIK-deleted or cIAP2 overexpressing SVEC cells (Supplemental Figure 3D).

Cells were treated with ABT-737 in the presence of caspase inhibitor and NF-κB activity was assayed by measuring nuclear translocation of NFκB p65 (Figure 4C, Supplemental Figures 3E and 3F). Following NIK deletion or cIAP2 over expression, NF-κB activation was strongly suppressed in response to ABT-737/Q-VD-OPh treatment (Figure 4C, Supplemental Figures 3E and 3F). ABT-737/Q-VD-OPh-dependent *Tnf* mRNA up-regulation was also inhibited in NIK deleted or cIAP2 overexpressing cells (Figure 4D). Finally, ectopic cIAP2 expression inhibited up-regulation of NIK following ABT-737/Q-VD-OPh treatment (Figure 4E). NF-κB transcriptional activity typically occurs following activation of either the canonical or the non-canonical (alternative) pathway. Our results support canonical NF-κB activation following MOMP, however given the well-established association between NIK with non-canonical NF-κB activity, we investigated non-canonical NF-κB activity following MOMP. Consistent with non-canonical pathway activation following MOMP, increased NF-κB p100 to p52 processing was observed following ABT-737/QVD treatment (Supplemental Figure 3G). Nevertheless, inhibiting non-canonical NF-κB activity (by deleting p100 or RelB) did not block canonical NF-κB activation following MOMP (Supplemental Figures 3H - J). These data support a model that MOMP signals NF-κB activation in a manner analogous to SMAC-mimetics. We therefore investigated the dependence of these effects on endogenous SMAC and OMI (a mitochondrial protein that also binds IAP proteins upon MOMP). E1A/Ras transformed wild-type MEF or $SMAC^{-/-}$ $OMI^{-/-}$ MEFs were treated with a combination of ABT-737 and UMI-77 (MCL-1 inhibitor) to engage MOMP and cIAP1 levels were measured (Figure 4F) [16, 17]. cIAP1 was depleted to a similar extent in both cell lines, demonstrating that cIAP1 degradation neither requires SMAC or OMI. Similarly, combined knockdown of SMAC and OMI did not rescue cIAP1 or XIAP loss following ABT-737/Q-VD-OPh treatment (Supplemental Figure 3K). Accordingly, wild-type MEF and $SMAC^{-/-}$ $OMI^{-/-}$ MEF activated NF-κB to a similar extent following MOMP (Figure 4G). Besides SMAC and OMI, other mitochondrial proteins can bind IAP proteins [18, 19]. Because these could potentially mediate IAP degradation we investigated whether MOMP could trigger IAP degradation by a SMAC-like mechanism. XIAP or an XIAP point-mutant (XIAP ^{D214S}

^{E314S}) unable to bind SMAC were expressed in BCL-2 dependent HeLa cells, and cells were treated to undergo MOMP (Figure 4H) [20]. While XIAP was rapidly degraded following ABT-263/Q-VD-OPh treatment, the XIAP mutant unable to bind SMAC was completely stabilised. This supports a model whereby IAP proteins are degraded by a SMAC-like mechanism following MOMP leading to NIK and NF-κB activation.

Mitochondrial permeabilisation activates an NF-κB dependent pro-inflammatory response

We investigated whether mitochondrial permeabilisation could induce additional pro-inflammatory cytokines besides TNF. BCL-xL dependent SVEC cells were treated with ABT-737 +/- Q-VD-OPh and culture supernatant was assayed for cytokine levels (Figure 5A, Supplemental Figure 4A). Several cytokines tested including MCP-1, KC, IL-6, TNF and IL-12, were up-regulated following ABT-737 treatment dependent on caspase-inhibition (Figure 5A, Supplemental Figure 4A). To investigate the NF-κB dependence of this pro-inflammatory signature SVEC cells expressing IκB^{SR} were treated with ABT-737 together with Q-VD-OPh. NF-κB inhibition silenced most cytokines analysed following ABT-737/Q-VD-OPh treatment (Figure 5B, Supplemental Figure 4B). Similarly, qRT-PCR analysis also revealed NF-κB dependent transcriptional up-regulation of various cytokines following ABT-737/Q-VD-OPh treatment (Figure 5C). Pro-inflammatory cytokine up-regulation following MOMP was not inhibited in MLKL-deleted cells, demonstrating its necroptosis independence (Supplemental Figure 4C). Canonical NF-κB activity alone was required for MOMP-induced cytokine up-regulation (Supplemental Figures 4D - H). Importantly, mitochondrial permeabilisation has recently been found to trigger a type I interferon response dependent upon mitochondrial DNA (mtDNA) activating the cGAS/STING signalling pathway [21, 22]. We therefore asked whether MOMP-induced NF-κB activity also contributed to the interferon response. SVEC cells expressing IκB^{SR} were treated with ABT-737 together with Q-VD-OPh and an interferon response gene signature was assayed by qRT-PCR (Figure 5D). As controls, STING signalling was inhibited by CRISPR/Cas-9 STING deletion or by using mtDNA-depleted ρ^0 SVEC cells (Supplemental Figure 4I and 4J). Consistent with the findings

of others, inhibition of cGAS/STING signalling effectively blocked the interferon transcriptional response following MOMP (Supplemental Figure 4K and 4L) [21, 22]. Significantly, suppressing NF-κB activity by $I\kappa B^{SR}$ expression, also inhibited the interferon transcriptional response (Figure 5D). Given this, we investigated the relationship between MOMP-induced NF-κB and STING activities. NF-κB activity was measured by monitoring NF-κB p65 nuclear translocation following ABT-737/Q-VD-OPh treatment in STING deleted or ρ^0 SVEC cells (Figure 5E). MOMP induced NF-κB activity was unaffected in STING deleted and ρ^0 cells, demonstrating that MOMP induced NF-κB activity neither requires mtDNA nor STING. In agreement, cIAP1 was still degraded following MOMP in both ρ^0 and STING-deleted SVEC cells following ABT-737/Q-VD-OPh treatment (Figure 5F). Finally, we investigated whether MOMP dependent NF-κB transcriptional targets also required STING signalling. STING-deleted SVEC cells were treated with ABT-737 together with Q-VD-OPh and cytokine transcript levels were measured by qRT-PCR (Figure 5G). Interestingly, while some NF-κB dependent transcriptional targets were affected by STING-deletion (*Mcp-1, Tnf*) others (*Kc*, *Gm-csf*) were not (Figure 5G), highlighting a differential requirement for STING-activity following MOMP.

MOMP dependent NF-κB signalling within dying cells promotes macrophage activation

We next investigated whether engaging mitochondrial apoptosis versus CICD could elicit different paracrine effects. BCL-xL dependent SVEC cells were incubated with ABT-737 +/- Q-VD-OPh and culture supernatant was transferred to primary bone marrow derived macrophages (BMDMs). Macrophage activation towards an M1, pro-inflammatory or an M2, anti-inflammatory state was assayed by qRT-PCR for transcripts characteristic of either state (Figure 6A). Importantly, media from cells undergoing CICD promoted macrophage activation towards an M1-phenotype, as determined by an increase in M1-associated transcript levels, whereas no effect was observed using media from apoptotic cells (Figure 6A). Consistent with this, BMDMs incubated with media from cells undergoing CICD also displayed an increase in the M1-associated marker, CD86 (Figure 6B). Media transferred from SVEC cells

undergoing CICD following APAF-1 knockdown or caspase-9 deletion also activated macrophages towards an M1-phenotype (Figure 6C, Supplemental Figures 5A and 5B). These effects required MOMP but not necroptosis, since media transferred from ABT-737/Q-VD-OPh treated BAX/BAK deleted cells failed to activate macrophages whereas media from MLKL deleted cells still activated macrophages (Figure 6D, Supplemental Figures 5C and 5D). Significantly, NF-κB inhibition (through $I\kappa B^{SR}$ expression) completely prevented the ability of cells undergoing CICD to promote M1-polarisation (Figure 6E). Inhibiting MOMP-dependent NF-κB activation by deletion of NIK, NF-κB p65, NEMO or by cIAP2 overexpression also had inhibitory effects (Supplemental Figures 5E - 5H). These results demonstrate that the ability of CICD to promote M1-macrophage polarisation requires MOMP dependent NF-κB activity. Because M1-macrophages are associated with anti-tumourigenic properties [23] we asked if tumour cells undergoing CICD could also activate macrophages towards an M1-profile. Primary tumour cells were isolated from a *Myc*-driven mouse model of pancreatic ductal adenocarcinoma (PDAC) and treated with ABT-737 together with Q-VD-OPh. Consistent with MOMP-dependent transcriptional up-regulation, TNF and IFNβ transcript levels increased following treatment (Supplemental Figure 5I). Culture supernatant was transferred to primary BMDMs and macrophage activation state was determined by qRT-PCR and flow-cytometry (Figures 6F and 6G). Under CICD conditions, media from PDAC cells also promoted polarisation of macrophages towards an M1-state (Figures 6F and 6G). We investigated what factor(s) produced by cells undergoing CICD could promote macrophage activation, focusing initially on TNF. SVEC cells were treated to undergo CICD and media was transferred to wild-type macrophages +/- Enbrel or to BMDMs derived from *TNFR-1*$^{-/-}$ mice and macrophage activation was assessed (Supplemental Figures 5J and 5K). In both cases, TNF signalling inhibition abrogated but did not abolish macrophage activation. Given this, coupled to our finding and that of others [21, 22] that cells undergoing CICD produce IFNβ led us to carry out similar experiments in the presence of neutralising IFNβ antibody. IFNβ neutralisation either alone or in combination with Enbrel (to block TNF) also inhibited macrophage activation (Supplemental Figure 5L) to some extent, demonstrating that TNF and IFNβ

contribute to CICD-induced macrophage activation. These data show that apoptosis and CICD can exert differential paracrine effects. Importantly, cells undergoing CICD can promote macrophage inflammatory activation towards a potentially anti-tumourigenic phenotype that requires MOMP-driven NF-κB activity.

Caspase-independent cell death displays potent anti-tumourigenic effects

Our findings suggest that under caspase-deficient conditions, MOMP-dependent NF-κB activity could confer therapeutic benefit in cancer treatment. To test this, we performed tumour allograft and treatment experiments using the colorectal cancer line CT26. These cells are RIPK3 deficient, allowing investigation of anti-tumourigenic CICD effects in the absence of necroptosis [24]. CT26 cells were transduced with GFP-tBID 2A BCL-2 encoding retrovirus to generate a heterogeneous population of BH3-mimetic sensitive and resistant cells. These were either caspase-proficient or rendered deficient in MOMP-induced caspase activity through APAF-1 knockdown (Supplemental Figure 6A). BH3-mimetic treatment induced a similar extent of MOMP in the presence or absence of APAF-1 (Supplemental Figure 6A). Cells were subcutaneously injected into BALB/c mice as syngeneic hosts. Following tumourigenesis, mice were treated with the BH3-mimetic ABT-263 (the orally available bioequivalent of ABT-737) to induce either tumour-cell apoptosis or CICD (Supplemental Figure 6B). Caspase activity was only detectable under apoptotic conditions, as confirmed by immunohistochemical staining for active caspase-3 (Supplemental Figure 6C). Supporting our *in vitro* data, Luminex assay revealed increased systemic cytokine levels; the majority of them pro-inflammatory, under conditions where tumour-specific CICD had been engaged (Figure 7A, Supplemental Figure 6D). We next investigated immune cell infiltration into tumours after CICD induction or apoptosis. While total macrophage infiltration was similar following either CICD or apoptosis (Supplemental Figure 6E), areas of macrophage accumulation were prevalent in tumours permissive only for CICD (Supplemental Figure 6F). Importantly, highly granulated macrophages expressed significant levels of MHC-II but not CD206, where CICD had specifically been triggered, mirroring the *in vitro* pro-inflammatory status observed previously (Supplemental Figures 6G, 6H).

An increase in T-cell infiltration was specifically observed following engagement of tumour cell CICD (Figures 7B, 7C). Together with our previous results, these data argue that CICD may be more immunogenic than apoptosis. Based on this, we directly addressed a possible therapeutic benefit of engaging tumour-specific CICD compared with apoptosis. BCL-2-dependent control or APAF-1 knockdown CT26 were subcutaneously injected into BALB/c mice. Once tumours were established, mice were treated four times with ABT-263 over a two-week period and tumour growth was monitored (Figure 7D). In the presence of vehicle alone, APAF-1 knockdown tumours grew slower than their wild-type counterparts. Tumour growth was unaffected by ABT-263 engagement of apoptosis, however under CICD conditions, ABT-263 treatment led to a significant overall reduction in tumour growth (Figure 7D). Further analysis revealed complete regression in 50% of mice bearing APAF-1 knockdown tumours, following ABT-263 treatment (Figure 7E). These data show that engaging CICD in tumours elicits inflammatory and immune effects. Most importantly, CICD displays potent anti-tumour effects, frequently leading to complete tumour regression.

CICD anti-tumourigenic effects requires NF-κB and intact immunity

Because engaging tumour CICD can lead to complete tumour regression, we investigated the role of immunity in mediating these effects. Similar to before, BCL-2-dependent control or APAF-1 knockdown CT26 were subcutaneously injected into BALB/c mice. Following tumour establishment, mice were treated four times with ABT-263 over a two-week period. Tumours were isolated at a defined endpoint, then analysed by flow-cytometry for tumour infiltrating immune cells. Tumours displaying regression or outgrowth, were termed as responders or non-responders respectively. Consistent with earlier results, APAF-1 knockdown tumours displayed the most effective response following ABT-263 treatment (Supplemental Figure 7A). Importantly, ABT-263 treatment led to an increase in total macrophage infiltration ($F4/80^{+}$) as well as an enhancement of activated, anti-tumourigenic macrophage subsets ($NOS2^{+}$, $CD86^{+}$, $MHC\text{-}II^{+}$) in tumours responding to CICD ($APAF\text{-}1^{SH}$)(Figure 8A and Supplemental Figure 7B). Analysis of tumour infiltrating T-cells, revealed an

increase in total T-cell infiltrate, comprised of increased $CD4^+$ T-helper cells and cytotoxic $CD8^+$ T-cells specifically in tumours responding to CICD (APAF-1^{SH})(Supplemental Figure 7C). Furthermore, an increase in $IFN\gamma^+$ $CD4^+$ T-helper cells, consistent with activation an anti-tumourigenic Th1 response, and activated cytotoxic $CD8^+$ cells ($IFN\gamma^+$, $GZMB^+$, $IFN\gamma^+/GZMB^+$) was identified in tumours responding to CICD (Figures 8B and 8C). These results demonstrate that an anti-tumourigenic immune activation correlates with response following CICD engagement. We therefore hypothesized that the beneficial effects of engaging CICD might be due to an ability of the immune system to control tumour growth. To test this, BCL-2-dependent control or APAF-1 knockdown CT26 cells were subcutaneously injected into immunocompromised NOD *scid* gamma $c^{-/-}$ (NSG) mice. Following tumour establishment, mice were left untreated or repeatedly treated with ABT-263 and tumour growth was monitored (Figure 8D and Supplemental Figure 7D). Importantly, ABT-263 treatment had no effect on tumour growth in NSG mice thereby supporting a key role for the immune system in mediating the anti-tumorigenic effects of CICD. APAF-1 knockdown tumours grew with similar kinetics to wild-type tumours in NSG mice (Supplemental Figure 7D), unlike their slower growth in immuncompetent BALB/c mice (Figure 7D). This may be due to a basal level of CICD activating, growth-inhibitory anti-tumour immunity. We carried out similar experiments under T-cell depleted conditions. BCL-2-dependent APAF-1 knockdown CT26 were subcutaneously injected into BALB/c mice. Once tumours were established, mice were treated with ABT-263 and T-cell depleting antibody (anti-Thy.1) or isotype control over a two-week period and tumour growth was monitored. Anti-Thy.1 treatment effectively depleted T-cells (Supplemental Figures 7E and 7F) and robustly inhibited the anti-cancer effects of engaging CICD, completely prevented tumour regression (Figure 8E and Supplemental Figure 7G). We addressed whether the anti-cancer effects of engaging CICD were dependent upon MOMP-induced NFκB activation. NF-κB proficient (vector) and deficient ($NEMO^{SH}$) BCL-2-dependent APAF-1 knockdown CT26 were subcutaneously injected into BALB/c mice (Supplemental Figure 7H). Following tumour formation, mice were treated with the BH3-mimetic ABT-263 to induce tumour-cell CICD and tumour

growth monitored (Figure 8F). Importantly, while ABT-263 CICD engagement promoted complete tumour regression, blocking NF-κB signalling through NEMO-knockdown, inhibited these effects (Figure 8F, Supplemental Figure 7I). Finally, we examined the potential clinical relevance of our findings by interrogating the Cancer Proteome Atlas (TCPA) [25]. We investigated the relationship between NF-κB, caspase activity and treatment outcome in renal cell carcinoma. Phospho-NF-κB p65 ^{S536} and cleaved-caspase 7 were used as measures of NFκB and caspase activity (Figure 8G). In line with our data, an inverse correlation between NF-κB activity and caspase-7 activity was found (Figure 8G). Importantly, high levels of NF-κB activity and low levels of caspase-7 activity also correlated with improved prognosis following therapy (Figure 8G). These data show that CICD is an immunogenic form of cell death, and that both NF-κB activity during CICD and immunity are required for its anti-tumourigenic effects.

Discussion

As others have reported [26], progressive mitochondrial dysfunction that ensues post-MOMP under caspase-inhibited conditions, leads to cell death. Nevertheless, our data demonstrates that how MOMP kills - either by apoptosis or CICD - has profoundly different effects. Unlike mitochondrial apoptosis, cells undergoing CICD display a pro-inflammatory phenotype dependent on NF-κB activity in the dying cell. Importantly, recent studies have shown that MOMP can also activate cGAS/STING signalling dependent on mtDNA [21, 22]. While we find that MOMP-dependent NF-κB activation and cGAS/STING signalling are independent events, both are required for the collective pro-inflammatory effects of CICD.

How does MOMP activate NF-κB? From our data we propose a model that MOMP activates NF-κB in a manner similar to small-molecule SMAC-mimetics. NF-κB is typically anti-apoptotic[27], moreover IKK activity can also promote survival through NF-κB-independent means[28]. Nevertheless, because widespread MOMP represents a terminal event, NF-κB or IKK activation post- MOMP won't allow long-term cell survival. Our results demonstrate that NIK-dependent canonical NF-κB activity is

important for the inflammatory and anti-tumour effects we observe. While NIK is best associated with activation of non-canonical NF-κB activity it has also been shown to crosstalk with canonical NF-κB activity [29-31]. Indeed, SMAC-mimetics also activate canonical NF-κB signalling in a manner that can depend on NIK [14, 15, 32]. The failure of NIK-deletion to completely prevent NF-κB signalling following MOMP suggests additional MOMP-dependent pathways may also signal NFκB activity.

Importantly, triggering CICD but not apoptosis often led to complete tumour regression. Especially under conditions of partial therapeutic response, as our experiments mimic, these data suggest that triggering tumour-specific CICD rather than apoptosis may be a more effective way to treat cancer. Indeed others have also observed enhanced anti-tumourigenic effects treated with cytotoxic agents together with caspase inhibitor [33, 34]. Why might CICD be more anti-tumourigenic than apoptosis? From our data, we reason that CICD is more immunogenic than apoptosis and that this contributes to its increased anti-tumour activity. Mirroring our findings, NF-κB activity has recently been shown to be a key immunogenic determinant of necroptotic cell death that is essential for anti-tumour immunity [35]. While necroptosis is not important for the anti-tumour effects of CICD, NF-κB activation is. Because many cancers are resistant to necroptosis[36], this significantly broadens the potential utility of targeting CICD in cancer. Importantly, caspase activity is neither required for MOMP-dependent cell death and indeed can have unwanted effects [4]. Coupled to our own findings, we propose that engaging CICD as a means of anti-cancer therapy warrants further investigation.

Acknowledgements

This work was supported by a Cancer Research UK Programme Foundation award (C40872/A20145)(S.T.) and a Cancer Research UK studentship. J.L. was supported, in part, by the University of Lyon and by fellowships from Fondation ARC pour la Recherche sur le Cancer and Hospices Civils de Lyon. G.I. was supported by an EMBO long-term postdoctoral fellowship (ALTF 55–2013). C.R-P. was supported by the Fondation ARC pour la Recherche sur le Cancer and the Agence Nationale de la Recherche (LABEX SIGNALIFE ANR-11-LABX-0028-01). We thank Drs. John Silke, Miguel Martins, Feng Zhang, Daniel Murphy and Damian Graczyk for reagents, Andrew Keith, Billy Clark, Tom Gilbey, Margaret O'Prey (Beatson Institute) Diane Vaughan, Laura Lapienyte, Véronique Imbert (Université de Nice-Sophia-Antipolis) Monica Hou and Catriona Thompson (University of Glasgow) for technical assistance. We acknowledge support from Cancer Research UK Glasgow Centre (C596/A18076), the Histology and BSU facilities at the Cancer Research UK Beatson Institute (C596/A17196) and Centre Méditerranéen de Médecine Moléculaire animal facility. Finally, we thank Catherine Winchester (Beatson Institute) for and members of the Tait lab reviewing the manuscript.

Author Contributions

E.G. and S.W.G.T. conceived the study, and designed the work-plan together with K.B., J.E.R and S.M. Experimental work: E.G., B.Z., S.D., F.B., C.C., K.C., A.R., J.L., G.I., E.P., N.Y. Development and contribution of reagents C.R-P., L.F., E.W., D.L., S.O., L.T., N.P., D.L., L.M., H.W., A.O. Data analysis: E.G., B.Z., S.D., F.B., K.C., A.R., J.L., G.I., E.P., K.R., K.B., J-E.R, S.W.G.T. Intellectual input: E.G., N.Y., M.A., A.O., J-E.R, K.B., S.W.G.T. Manuscript writing: E.G. and S.W.G.T.

Figure 1. Mitochondrial permeabilisation can engage necroptosis as a form of CICD

(A) SVEC cells were treated with ABT-737 (10 μM) +/- Q-VD-OPh (10 μM) and immunoblotted for PARP and β-Actin. Representative images from three independent experiments.

(B) SVEC cells were treated for 72 h with ABT-737 (10 μM) +/- caspase inhibitor Q-VD-OPh (10 μM). For (B)(C)(D) and (E) cell viability was measured by flow-cytometry and PI exclusion. n=5 independent experiments.

(C) SVEC cells stably expressing LZRS empty vector (vector) or LZRS-MCL-1 were treated for 72 h with ABT-737 (10 μM) +/- Q-VD-OPh (10 μM). *n*=3 independent experiments; mean values ± S.E.M

(D) Control or RIPK3^{SH} SVEC cells were treated for 72 h with TNF (20 ng/ml) +/- caspase inhibitor zVAD-FMK (50 μM) and/or RIPK1 inhibitor necrostatin-1 (30 μM). *n*=3 independent experiments; mean values ± S.E.M

(E) SVEC cells stably expressing pLKO empty vector (vector) or pLKO-shRIPK3 (RIPK3^{SH}) were treated for 72 h with ABT-737 (10 μM) +/- caspase inhibitor Q-VD-OPh (10 μM) and/or RIPK1 inhibitor necrostatin-1 (30 μM). *n*=3 independent experiments; mean values ± S.E.M.

(F) BCL-xL dependent SVEC cells expressing empty vector (pLKO1) or pLKO-shAPAF-1 (APAF-1^{SH}) were treated for 24 h with ABT-737 (10 μM) +/- caspase inhibitor Q-VD-OPh (30 μM). For (F)(H)(I)(J) cell death was measured using an IncuCyte imager, measuring SYTOX Green uptake. *n*=3 independent experiments; mean values ± S.E.M.

(G) BCL-xL dependent SVEC cells were treated with ABT-737 (10 μM) +/- Q-VD-OPh (30 μM) then immunoblotted for indicated proteins. Representative images from three independent experiments.

(H) BCL-xL dependent SVEC cells stably expressing an empty vector (pLKO1) or pLKO1-shRIPK3 (RIPK3^{SH}) were treated with ABT-737 (10 μM) in the presence of caspase inhibitor Q-VD-OPh (30 μM) and/or necrostatin-1 (30 μM). A representative time-point shown (16 h). *n*=5 independent experiments; mean values ± S.E.M.

(I) Control or MLKL-deleted BCL-xL dependent SVEC cells were treated with TNF (20 ng/ml) and zVAD-FMK (50 μM) +/- necrostatin-1 (30 μM). A representative time-point is shown (21 h). *n*=3 independent experiments; mean values ± S.E.M.

(J) Control (vector^{CRISPR}) or MLKL-deleted (MLKL^{CRISPR}) BCL-xL dependent SVEC cells were treated with ABT-737 (10 μM) together with Q-VD-OPh (30 μM) and/or necrostatin-1 (30 μM). A representative time-point is shown (21 h). *n*=3 independent experiments; mean values ± S.E.M.*p<0.05, **p<0.01, ***P<0.001; Holm-Sidak-corrected one way ANOVA (B), two-tailed unpaired t-test (C, D, E, H, I, J).

Figure 2. MOMP induces TNF-synthesis under caspase-deficient conditions

(A) SVEC cells were treated (72 h) with ABT-737 (10 μM) +/- Q-VD-OPh (10 μM) necrostatin-1 (30 μM) or Enbrel (50 μg/ml). Cell viability was measured by flow-cytometry (%PI^+ cells). *n*=3 independent experiments; mean values ± S.E.M.

(B) BCL-xL dependent SVEC cells were treated for 22 h with ABT-737 (10 μM) together with Q-VD-OPh (10 μM) or necrostatin-1 (30 μM) +/- Enbrel (50 μg/ml). cell death was measured using an IncuCyte imager, measuring SYTOX Green uptake. *n*=3 independent experiments; mean values ± S.E.M

(C) BCL-xL dependent control or RIPK3 shRNA SVEC cells were treated as indicated with ABT-737 (10 μM), Q-VD-OPh (30 μM) and/or necrostatin-1 (30 μM), in the presence of TNF (20 ng/ml). Cell death was measured by IncuCyte imager, using SYTOX Green uptake, a representative time-point is shown (16 h). *n*=3 independent experiments; mean values ± S.E.M.

(D) BCL-xL dependent SVEC cells were treated with ABT-737 (10 μM) +/- Q-VD-OPh (30 μM) and *Tnf* expression was measured by qRT-PCR. Data represent mean of triplicate samples and is representative of three independent experiments.

(E) Control ($vector^{CRISPR}$) or BAX/BAK deleted BCL-xL dependent SVEC cells (BAX/BAK^{CRISPR}) were treated with ABT-737 (10 μM) and Q-VD-OPh (30 μM) then *Tnf* expression was measured by qRT-PCR. Data represent the mean of triplicate samples and are representative of three independent experiments.

(F) BCL-xL dependent SVEC cells were treated with ABT-737 (10 μM) together with Q-VD-OPh (30 μM). Media TNF levels were measured by ELISA. *n*=3 independent experiments; mean values ± S.E.M.

(G) BCL-xL dependent SVEC cells expressing APAF-1 shRNA ($APAF\text{-}1^{SH}$) were treated with ABT-737 (10 μM) and *Tnf* expression was measured by qRT-PCR.

(H) Control or Caspase-9 deleted BCL-xL dependent SVEC cells were treated with ABT-737 (10 μM) and *Tnf* expression was measured by qRT-PCR.

(I) BCL-xL dependent E1A/Ras transformed MEFs were treated as in (D) and *Tnf* expression was measured by qRT-PCR. For (G)(H)(I) data represent the mean of triplicate samples and are representative of three independent experiments. *p<0.05, **p<0.01, ***P<0.001; two-tailed unpaired t-test (A, B) Holm-Sidak-corrected one way ANOVA (F). Statistical source data can be found in Supplementary Table 5.

Figure 3. Mitochondrial permeabilisation activates NF-κB

(A) BCL-xL dependent SVEC cells were treated with ABT-737 (10 μM) +/- Q-VD-Oph (30 μM) for 1 h, immunostained for p65 and analysed by confocal microscopy. TNF (20 ng/ml) was used as positive control for p65 nuclear translocation. Scale bar represents 30μM. Representative images from three independent experiments.

(B) Quantification of cells (from A) displaying nuclear p65, minimum 300 cells were counted per condition. Ctrl: *n*=15 individual fields, ABT-737: *n*=15 individual fields, ABT-737/QVD: *n*=18, individual fields TNF: *n*=15 individual fields ± SEM.

(C) BCL-xL dependent SVEC cells deleted for BAX and BAK (BAX/BAK^{CRISPR}) or cells expressing empty vector (vector^{CRISPR}) were treated with ABT-737 (10 μM) +/- Q-VD-OPh (30 μM) for 6 h then immunostained for p65 and cytochrome *c*. Scale bar represents 30μM. Representative images from three independent experiments.

(D) Quantification of cells in (C) displaying nuclear p65, minimum 300 cells were counted per condition. Vector^{CRISPR}-ctrl: *n*=15 individual fields, vector^{CRISPR}-ABT-737/QVD: *n*=16 individual fields, BAX/BAK^{CRISPR}-ctrl: *n*=15 individual fields, BAX/BAK^{CRISPR} -ABT-737/QVD: *n*=16 individual fields ± SEM.

(E) BCL-xL dependent SVEC cells were treated with ABT-737 (10 μM) +/- Q-VD-OPh (30 μM) and blotted for p-IκBα, total IκBα and β-Actin. .Representative image of three independent experiments.

(F) BCL-xL dependent SVEC cells transiently expressing two different NFκB reporters (PGL3-TNF reporter 1 or PGL3-NP3 reporter 2 were treated with ABT-737 (10 μM) +/- Q-VD-OPh (30 μM) for 3 h and luciferase reporter assay was performed. Data represent the mean of duplicate samples and are representative of three independent experiments.

(G) BCL-xL dependent SVEC cells stably expressing IκB^{SR} or empty vector (PMX) were treated with ABT-737 (10 μM) together with Q-VD-OPh (30 μM) or TNF (20 ng/ml) for 1 h and then immunostained for p65, minimum 300 cells were counted per condition. Quantification of cells displaying nuclear p65 was performed. Vector-ctrl: *n*=15 individual fields, vector-ABT-737/QVD: *n*=18 individual fields, vector-TNF/QVD: *n*=16 individual fields, IκB^{SR}-ctrl: *n*=15 individual fields, IκB^{SR}-ABT-737/QVD: *n*=15 individual fields, IκB^{SR}-TNF/QVD: *n*=15 individual fields ± SEM.

(H) BCL-xL dependent SVEC cells stably expressing IκB^{SR} or empty vector (PMX) were treated with ABT-737 (10 μM) and Q-VD-OPh (30 μM) and *Tnf* expression was measured by qRT-PCR. Data represent the mean of triplicate samples and are representative of three independent experiments.

*p<0.05, **p<0.01, ***P<0.001; Tukey-corrected one way ANOVA (B), Tukey-corrected two way ANOVA (D, G).

Statistical source data can be found in Supplementary Table 5. Unprocessed original scans of blots are shown in Supplementary Figure 9. .

Figure 4. MOMP activates NF-κB through IAP down-regulation and NIK activation

(A) Cell lysates from BCL-xL dependent SVEC cells treated with SMAC-mimetic (SM-83, 50 nM) or ABT-737 (10 μM) and Q-VD-OPh (30 μM, 8h) were immunoblotted for indicated proteins. Representative image of three independent experiments.

(B) Control or BAX/BAK deleted BCL-xL dependent SVEC cells were treated with ABT-737 (10 μM) and Q-VD-OPh (30 μM). Cell lysates were immunoblotted for indicated proteins. Representative images of three independent experiments.

(C) Control, NIK-deleted or cIAP2 overexpressing BCL-xL dependent SVEC cells were treated with ABT-737 (10μM) and Q-VD-OPh (30 μM, 6h) and immunostained for p65, minimum 300 cells were counted per condition. Quantification depicts the percentage nuclear p65 positive cells. Vector^{CRISPR}-ctrl: *n*=15 individual fields, vector^{CRISPR}-ABT-737/QVD: *n*=18 individual fields, NIK^{CRISPR}-ctrl: *n*=16 individual fields, NIK^{CRISPR}-ABT-737/QVD: *n*=18 individual fields, vector-ctrl: *n*=15 individual fields, vector-ABT-737/QVD: *n*=18 individual fields, cIAP2-ctrl: *n*=15 individual fields, cIAP2-ABT-737/QVD: *n*=20 individual fields ± SEM.

(D) Control, NIK-deleted or cIAP2 overexpressing BCL-xL dependent SVEC cells were treated with ABT-737 (10 μM) and Q-VD-OPh (30 μM) for 6h. *Tnf* expression was measured by qRT-PCR. Data represent the mean of triplicate samples and are representative of three independent experiments.

(E) Control or cIAP2 overexpressing BCL-xL dependent SVEC cells were treated with ABT-737 (10 μM) and Q-VD-OPh (30 μM) as indicated and immunoblotted for NIK and β-Actin. Representative image of three independent experiments.

(F) Wild-type or SMAC/OMI$^{-/-}$ E1A/ras transformed MEFs were treated with ABT-737 (10 μM) and UMI-77 (10 μM) and Q-VD-OPh (30 μM) for 4 h. Cell lysates were immunoblotted for indicated proteins. Representative image of three independent experiments.

(G) Wild-type or SMAC/OMI$^{-/-}$ E1A/ras transformed MEFs were treated with ABT-737 (10 μM), UMI-77 (10 μM) and Q-VD-OPh (30 μM)(8h) then immunostained for cytochrome *c* and p65. Cells that had undergone MOMP were scored for nuclear p65 translocation, minimum 300 cells counted per condition. WT and SMAC/OMI$^{-/-}$-ctrl: *n*=15 individual fields, wt and SMAC/OMI$^{-/-}$-ABT-737/UMI-77/QVD: n=18 individual fields ± SEM.

(H) BCL-2 dependent HeLa cells or cells transiently expressing TRAF2 together with either wild-type XIAP or XIAP BIR3 mutant (D214S E314S) were treated with ABT-263 (10 μM) and Q-VD-OPh (30 μM) for 4 h. Cell lysates were blotted for XIAP and β-Actin. Representative image of three independent experiments. Densitometric quantification of Western blots was performed. *n* = 3 independent experiments; mean values ± S.E.M.. *p<0.05, **p<0.01, ***P<0.001; Tukey-corrected two way ANOVA (C, G, H). Statistical source data can be found in Supplementary Table 5. Unprocessed original scans of blots are shown in Supplementary Figure 9.

Figure 5. Mitochondrial permeabilisation initiates an NF-κB dependent pro-inflammatory response

(A) BCL-xL dependent SVEC cells were treated with ABT-737 (10 μM) and Q-VD-OPh (30 μM) for 8h. Conditioned media was analysed for cytokine detection using Luminex assay. Data represents the mean of duplicate samples and is representative of two independent experiments.

(B) BCL-xL dependent SVEC cells stably expressing $I\kappa B^{SR}$ or empty vector (vector) were treated with ABT-737 (10 μM) and Q-VD-OPh (30 μM) for 8h. Conditioned media was then analysed for cytokine levels using Luminex assay. Data is the mean of duplicate samples and is representative of two independent experiments.

(C) BCL-xL dependent SVEC cells stably expressing $I\kappa B^{SR}$ or empty vector (PMX) were treated with ABT-737 (10 μM) and Q-VD-OPh (30 μM) for 6 h and mRNA levels of *Mcp-1*, *Kc*, *Gm-csf and Tnf* were measured by qRT-PCR.

(D) BCL-xL dependent SVEC cells stably expressing $I\kappa B^{SR}$ or PMX empty vector (vector) with ABT-737 (10 μM) and Q-VD-OPh (30 μM) for 8 h and *Ifnβ, Irf7* and *Oasl1* were measured by qRT-PCR.

(E) BCL-xL dependent SVEC cells deleted for STING ($STING^{CRISPR}$) or cells expressing empty vector ($vector^{CRISPR}$), as well as ρ^0 cells were treated with ABT-737 (10 μM) and Q-VD-OPh (30 μM) for 6 h, immunostained for p65 and analysed by confocal microscopy. Quantification includes the percentage of cells with nuclear p65, minimum 300 cells (left graph) and 240 cells (right graph) counted per condition. $Vector^{CRISPR}$, $STING^{CRISPR}$-ctrl and ABT-737/QVD: *n*=15 individual fields , $vector^{CRISPR}$ and $STING^{CRISPR}$-TNF: *n*=11 individual fields, untreated and EtBr-ctrl and ABT-737/QVD: *n*=22 individual fields, untreated and EtBr-TNF: *n*=9 individual fields ± SEM.

(F) BCL-xL dependent SVEC cells deleted for STING ($STING^{CRISPR}$) or expressing empty vector ($vector^{CRISPR}$) and ρ^0 SVEC were treated as indicated and cell lysates were immunoblotted for cIAP1, XIAP and β-Actin. Representative image from three independent experiments.

(G) BCL-xL dependent SVEC cells deleted for STING ($STING^{CRISPR}$) or expressing empty vector ($vector^{CRISPR}$) were treated with ABT-737 (10 μM) and Q-VD-OPh (30 μM) for 6 h and mRNA levels of *Mcp-1*, *Kc*, *Gm-csf and Tnf* were measured by qRT-PCR. For (C), (D)and (G) data represent the mean of triplicate samples and are representative of three independent experiments.

*p<0.05, **p<0.01, ***P<0.001; Tukey-corrected two way ANOVA (E). Statistical source data can be found in Supplementary Table 5. Unprocessed original scans of

blots are shown in Supplementary Figure 9. .

Figure 6. MOMP dependent NF-κB activity promotes macrophage activation

(A) Bone marrow-derived macrophages (BMDMs) were incubated overnight with conditioned media (CM) from BCL-xL dependent SVEC cells that had been treated with ABT-737 (10 μM) – CM (APO)- or ABT-737 (10 μM) and Q-VD-OPh (30 μM) – CM (CICD)- for 8 h. Expression of indicated M1 and M2 markers was determined by qRT-PCR.

(B) BMDMs were treated as in (A) and stained for either M1 ($CD86^+$) or M2 ($CD206^+$) surface markers. *n*=3 independent experiments; mean values ± S.E.M.

(C) BMDMs were incubated overnight with conditioned media (CM) from vector or APAF-1 knockdown BCL-xL dependent SVEC cells that had been treated with ABT-737 (10 μM) for 8 h. qRT-PCR was performed on BMDMs to assess M1 marker expression.

(D) BMDMs were incubated overnight with conditioned media (CM) from control or BAX/BAK deleted BCL-xL dependent SVEC cells that had been treated with ABT-737 (10 μM) and Q-VD-OPh (30 μM) for 8 h. qRT-PCR was performed on BMDMs to assess M1 marker expression.

(E) BMDMs were incubated overnight with conditioned media (CM) from vector or $IκB^{SR}$ overexpressing BCL-xL dependent SVEC cells that had been treated with ABT-737 (10 μM) and Q-VD-OPh (30 μM) for 8 h. qRT-PCR was performed on BMDMs to assess M1 marker expression.

(F) BMDMs were incubated overnight with conditioned media (CM) from murine primary pancreatic tumour cells (Myc-PDAC) that had been treated for 24 h with ABT-737 (10 μM) +/- Q-VD-OPh (10 μM). M1/M2 status was assessed with qRT-PCR.

(G) BMDMs were incubated overnight with conditioned media (CM) transferred from murine primary pancreatic tumour cells (Myc-PDAC) that have been treated for 24 h with ABT-737 (10 μM) +/- Q-VD-OPh (10 μM). The activation profile was measured by FACS, staining for either M1 surface marker ($CD86^+$) or M2 surface marker ($CD206^+$). *n*=3 independent experiments; mean values ± S.E.M. For (A)(C)(D)(E)(F) data represent the mean of triplicate samples and are representative of three independent experiments.

*p<0.05, **p<0.01, ***P<0.001; Tukey-corrected one way ANOVA (B, G). Statistical source data can be found in Supplementary Table 5.

Figure 7. CICD displays enhanced anti-tumorigenic effects versus apoptosis

(A) Control (pLKO1) or APAF-1 knockdown (APAF-1^{SH}) BCL-2 dependent CT26 cells were injected subcutaneously into Balb/C mice ($5x10^5$ cells/mouse). Following tumour formation, mice were treated with either vehicle or ABT-263 (100mg/kg) for 2 times over a 7-day period then sacrificed one-day post-final treatment. Serum levels of the indicated cytokines were measured by Luminex assay. *n*=3 independent experiments; mean values ± S.E.M.

(B) Representative immunohistochemistry images (n=3 mice) of CD3 staining (T cells), taken from control (pLKO1) or pLKO1-shAPAF-1 (APAF-1^{SH}) BCL-2 dependent CT26 cell tumour sections, following vehicle or ABT-263 (100mg/kg) treatment, 2 times in a week. Scale bar represents 100μM.

(C) Control (pLKO1) or pLKO1-shAPAF-1 (APAF-1^{SH}) BCL-2 dependent CT26 cells were injected subcutaneously into Balb/C mice. Following tumour formation, mice were treated with vehicle or ABT-263 for 2 times in a 7-day period and sacrificed one day post-final treatment. T cell tumour infiltration was measured by flow-cytometry ($CD3^+DAPI^-$ cells). Vector-vehicle and ABT-263, APAF-1^{SH}-vehicle: *n*=9 mice, APAF-1^{SH}-ABT-263: *n*=8 mice ± SD.

(D) BCL-2 dependent CT26 cells (wt vs APAF-1^{SH}) were injected into mice and treated with either vehicle or ABT-263 (100mg/kg) 2 times/week for a total of two weeks. Tumour growth was determined every 2 days by measuring the tumour volume (mm^3). WT-vehicle, APAF-1^{SH}-vehicle and ABT-263: *n*= 10 mice, wt-ABT-263: *n*=9 mice ± SEM from one experiment, repeated independently. Arrows indicate time of treatment.

(E) Individual mouse tumour growth from (D) is shown. Post-treatment, each individual tumour was normalized (%) to the initial volume (mm^3) obtained the first day of treatment (100% normalized tumour volume). Arrows indicate time of treatment.

*p<0.05, **p<0.01, ***P<0.001; Tukey-corrected two way ANOVA (C, D).

Figure 8. CICD anti-tumourigenic effects requires NF-κB and intact immunity

(A) Vector or APAF-1^{SH} BCL-2 dependent CT26 cells were injected into Balb/C mice. Tumour bearing mice were treated with vehicle or ABT-263 (4 times over 2 weeks). Mice were sacrificed at day 13 post-treatment and split into responder (R) and non-responder (NR) groups. Total macrophage tumour infiltration ($F4/80^{+}$) and M1-like macrophage activation status ($NOS2^{+}$, $CD86^{+}$ and $MHC\text{-}II^{+}$) was measured by flow cytometry.

(B) Samples generated in 8A were analysed for tumour-infiltrating activated $CD4^{+}$ T cells ($IFN\gamma^{+}$).

(C) Samples generated in 8A were analysed for tumour-infiltrating activated $CD8^{+}$ T cells ($IFN\gamma^{+}$). For A-C The number of live infiltrated immune cells were measured by FACS and subsequently normalized to total live tumour cells and tumour weight. Data represents the mean ± SD of tumours; n=6-9 mice per group (individual n number per sub-group is provided in the figure).

(D) BCL-2 dependent APAF-1^{SH} CT26 cells were injected into NSG mice. Tumour bearing mice were treated with vehicle or ABT-263. Data represents the mean ± SD of tumour volume (mm^3). Arrows indicate treatment points; n=10 mice per group.

(E) BCL-2 dependent APAF-1^{SH} CT26 cells were injected into Balb/C mice. Tumour bearing mice were pre-treated with isotype control or anti-Thy.1. One day later mice were treated with vehicle or ABT-263 (black arrows indicate treatment points) together with isotype control or anti-Thy.1 (red arrows indicate treatment points). Tumour growth was monitored every other day. APAF-1^{SH} + Isotype ctrl + ABT-263: *n*=10 mice, APAF-1^{SH} + anti-Thy.1 + ABT-263: *n*=9 mice ± SEM.

(F) BCL-2 dependent APAF-1^{SH} CT26 cells and expressing vector or NEMO shRNA were injected into mice. Tumour bearing mice were treated with vehicle or ABT-263. Individual mouse tumour growth is shown. Post-treatment, each tumour was normalized (%) to the initial tumour volume (each set at 100%). Arrows indicate time of treatment and asterisks tumours that grew over 500% of the initial volume. APAF-1^{SH}-vector + vehicle: *n*=9 mice, APAF-1^{SH}-vector + ABT-263: *n*=10 mice, APAF-1^{SH}-$NEMO^{SH}$ + vehicle: *n*=8 mice, APAF-1^{SH}-$NEMO^{SH}$ + ABT-263: *n*=8 mice.

(G) *In silico* analysis of clinical data from renal cell carcinoma patients using the TCPA database.

*p<0.05, **p<0.01, ***P<0.001; Dunn's-corrected Kruskal-Wallis (A, B, C), Tukey-corrected two way ANOVA (E), Spearman's rank test (correlation), Cox and Log-Rank test (Kaplan Meier curves) (G).

References

1. Tait, S.W. & Green, D.R. Mitochondria and cell death: outer membrane permeabilization and beyond. *Nat Rev Mol Cell Biol* **11**, 621-632 (2010).
2. Tait, S.W., Ichim, G. & Green, D.R. Die another way--non-apoptotic mechanisms of cell death. *J Cell Sci* **127**, 2135-2144 (2014).
3. Lopez, J. *et al.* Mito-priming as a method to engineer Bcl-2 addiction. *Nat Commun* **7**, 10538 (2016).
4. Ichim, G. & Tait, S.W. A fate worse than death: apoptosis as an oncogenic process. *Nat Rev Cancer* **16**, 539-548 (2016).
5. Labi, V. & Erlacher, M. How cell death shapes cancer. *Cell Death Dis* **6**, e1675 (2015).
6. Ichim, G. *et al.* Limited mitochondrial permeabilization causes DNA damage and genomic instability in the absence of cell death. *Mol Cell* **57**, 860-872 (2015).
7. Lovric, M.M. & Hawkins, C.J. TRAIL treatment provokes mutations in surviving cells. *Oncogene* **29**, 5048-5060 (2010).
8. Liu, X. *et al.* Caspase-3 promotes genetic instability and carcinogenesis. *Mol Cell* **58**, 284-296 (2015).
9. Tait, S.W. *et al.* Widespread mitochondrial depletion via mitophagy does not compromise necroptosis. *Cell Rep* **5**, 878-885 (2013).
10. Oltersdorf, T. *et al.* An inhibitor of Bcl-2 family proteins induces regression of solid tumours. *Nature* **435**, 677-681 (2005).
11. Wallach, D., Kang, T.B., Dillon, C.P. & Green, D.R. Programmed necrosis in inflammation: Toward identification of the effector molecules. *Science* **352**, aaf2154 (2016).
12. Kim, K.W. *et al.* Caspase cleavage product lacking amino-terminus of IkappaBalpha sensitizes resistant cells to TNF-alpha and TRAIL-induced apoptosis. *J Cell Biochem* **85**, 334-345 (2002).
13. Van Antwerp, D.J., Martin, S.J., Kafri, T., Green, D.R. & Verma, I.M. Suppression of TNF-alpha-induced apoptosis by NF-kappaB. *Science* **274**, 787-789 (1996).
14. Varfolomeev, E. *et al.* IAP antagonists induce autoubiquitination of c-IAPs, NF-kappaB activation, and TNFalpha-dependent apoptosis. *Cell* **131**, 669-681 (2007).
15. Vince, J.E. *et al.* IAP antagonists target cIAP1 to induce TNFalpha-dependent apoptosis. *Cell* **131**, 682-693 (2007).
16. Martins, L.M. *et al.* Neuroprotective role of the Reaper-related serine protease HtrA2/Omi revealed by targeted deletion in mice. *Mol Cell Biol* **24**, 9848-9862 (2004).
17. Abulwerdi, F. *et al.* A novel small-molecule inhibitor of mcl-1 blocks pancreatic cancer growth in vitro and in vivo. *Mol Cancer Ther* **13**, 565-575 (2014).
18. Verhagen, A.M. *et al.* Identification of mammalian mitochondrial proteins that interact with IAPs via N-terminal IAP binding motifs. *Cell Death Differ* **14**, 348-357 (2007).
19. Zhuang, M., Guan, S., Wang, H., Burlingame, A.L. & Wells, J.A. Substrates of

IAP ubiquitin ligases identified with a designed orthogonal E3 ligase, the NEDDylator. *Mol Cell* **49**, 273-282 (2013).
20. Silke, J. *et al.* The anti-apoptotic activity of XIAP is retained upon mutation of both the caspase 3- and caspase 9-interacting sites. *J Cell Biol* **157**, 115-124 (2002).
21. Rongvaux, A. *et al.* Apoptotic caspases prevent the induction of type I interferons by mitochondrial DNA. *Cell* **159**, 1563-1577 (2014).
22. White, M.J. *et al.* Apoptotic caspases suppress mtDNA-induced STING-mediated type I IFN production. *Cell* **159**, 1549-1562 (2014).
23. Biswas, S.K. & Mantovani, A. Macrophage plasticity and interaction with lymphocyte subsets: cancer as a paradigm. *Nat Immunol* **11**, 889-896 (2010).
24. Aaes, T.L. *et al.* Vaccination with Necroptotic Cancer Cells Induces Efficient Anti-tumor Immunity. *Cell Rep* **15**, 274-287 (2016).
25. Li, J. *et al.* TCPA: a resource for cancer functional proteomics data. *Nat Methods* **10**, 1046-1047 (2013).
26. Lartigue, L. *et al.* Caspase-independent mitochondrial cell death results from loss of respiration, not cytotoxic protein release. *Mol Biol Cell* **20**, 4871-4884 (2009).
27. Hayden, M.S. & Ghosh, S. NF-kappaB, the first quarter-century: remarkable progress and outstanding questions. *Genes Dev* **26**, 203-234 (2012).
28. Dondelinger, Y. *et al.* NF-kappaB-Independent Role of IKKalpha/IKKbeta in Preventing RIPK1 Kinase-Dependent Apoptotic and Necroptotic Cell Death during TNF Signaling. *Mol Cell* **60**, 63-76 (2015).
29. Ramakrishnan, P., Wang, W. & Wallach, D. Receptor-specific signaling for both the alternative and the canonical NF-kappaB activation pathways by NF-kappaB-inducing kinase. *Immunity* **21**, 477-489 (2004).
30. Zarnegar, B., Yamazaki, S., He, J.Q. & Cheng, G. Control of canonical NF-kappaB activation through the NIK-IKK complex pathway. *Proc Natl Acad Sci U S A* **105**, 3503-3508 (2008).
31. Demchenko, Y.N. *et al.* Classical and/or alternative NF-kappaB pathway activation in multiple myeloma. *Blood* **115**, 3541-3552 (2010).
32. Cheung, H.H. *et al.* SMG1 and NIK regulate apoptosis induced by Smac mimetic compounds. *Cell Death Dis* **2**, e146 (2011).
33. Kim, K.W., Moretti, L. & Lu, B. M867, a novel selective inhibitor of caspase-3 enhances cell death and extends tumor growth delay in irradiated lung cancer models. *PLoS One* **3**, e2275 (2008).
34. Werthmoller, N., Frey, B., Wunderlich, R., Fietkau, R. & Gaipl, U.S. Modulation of radiochemoimmunotherapy-induced B16 melanoma cell death by the pan-caspase inhibitor zVAD-fmk induces anti-tumor immunity in a HMGB1-, nucleotide- and T-cell-dependent manner. *Cell Death Dis* **6**, e1761 (2015).
35. Yatim, N. *et al.* RIPK1 and NF-kappaB signaling in dying cells determines cross-priming of CD8(+) T cells. *Science* **350**, 328-334 (2015).
36. Koo, G.B. *et al.* Methylation-dependent loss of RIP3 expression in cancer represses programmed necrosis in response to chemotherapeutics. *Cell Res* **25**, 707-725 (2015).

Methods

Cell lines, plasmids and reagents

SVEC, MEF, HeLa and primary Myc-PDAC cells were cultured in DMEM high glucose medium, CT26 cells were cultured in RPMI high glucose medium. Culture media were supplemented with 10% FCS, 2 mM glutamine, 1 mM sodium pyruvate, 50μM β-mercaptoethanol, penicillin (10000 units/mL) and streptomycin (10000 units/mL). Reagents (Supplemental Table 1) used were as follows: ABT-737, Q-VD-OPh, ABT-263 - APEX Bio, UMI-77 - Selleckchem, MG132 - Calbiochem, necrostatin-1 - Sigma, Enbrel - Pfizer, murine and human TNF - Peprotech, murine-CSF - Miltenyi Biotec -MACS, PMA - Sigma, Ionomycin-Santa Cruz, Brefeldin A – eBioscience, LEAF™ Purified anti-mouse IFN-β Antibody, LEAF™ Purified Armenian Hamster IgG Isotype control Antibody - Biolegend, collagenase - Sigma, SMAC-mimetic (SM-83) has been previously described [37]. Using pTIZ-cIAP2 and pBabe-puro-IκB^{SR} as template, cIAP2 and IκB^{SR} were cloned into PMX using PCR/restriction digest based cloning. For lentiviral transduction the following plasmids were used pLKO-puro, pLKO-RIPK3^{SH} (mouse SH-RNA, TRCN0000022535), pLKO1-blasti (mouse non-target control), pLKO1-blasti-APAF-1^{SH} (mouse SH-RNA, TRCN00000012278), pLKO-blasti-RIPK3^{SH} (mouse SH-RNA, TRCN00000022538), pLKO1-puro (non-target control), pLKO1-puro-APAF-1^{SH} (mouse SH-RNA, TRCN00000012278), pLKO1-blasti-NEMO^{SH} (mouse SH-RNA, TRCN0000088811) (Supplemental Table 2). The puromycin cassette in the pLKO1 vector was substituted with blasticidin cassette using PCR/restriction digest based cloning. For CRISPR/Cas9 based genome editing the following sequences were cloned into LentiCRISPRv1-puro (Addgene, 49535, [38]) targeting mouse Caspase-9: CTTCACGCGCGACATGATCG, mouse NIK: TCGCTGGCCAGCGATCGCTC, or LentiCRISPRv2-puro (Addgene, 52961, [39]), targeting mouse BAX: CAACTTCAACTGGGGCCGCG, mouse BAK: GCGCTACGACACAGAGTTCC, mouse STING: AGCGGTGACCTCTGGGCCGT, mouse IKKβ: TCACACATACCCCGTGACGG, mouse NEMO: TGGCCTTGTCCAACCAGCGG, mouse p65: ATCGAACAGCCGAAGCAACG, mouse p100/p52: AAGACAGCGGGTTCCGTGCG, mouse RelB: AGCGGCCCTCGCACTCGTAG, pRRL M1 Scramble CRISPR-Cas9-T2A-puro, pRRL M1 Scramble CRISPR-Cas9-T2A-puro-oligo sequence targeting mouse MLKL: GCACACGGTTTCCTAGACGC (Supplemental

Table 3). PEF-human XIAP wt-FLAG (C-ter) or PEF-human XIAP_D214S_E314S (BIR3 mutant)-FLAG (C-ter) provided by Dr. John Silke[20]. General reagents, siRNA/shRNA reagents, CRISPR targeting sequences and neutralising antibodies are also described in Supplemental Tables 1,2, 3 and 6 respectively. No cell lines were authenticated. Cell lines were tested multiple times over the study for mycoplasma contamination. No cell lines used in this study were found in the database of commonly misidentified cell lines that is maintained by ICLAC.

Retroviral and lentiviral transduction

Phoenix Eco (for retroviral transduction of mouse cell lines) and Phoenix Ampho (for human cells) were transfected with 5 µg of selected plasmids, using Lipofectamine 2000 (Invitrogen). After two days, the viral supernatant was filtered and used to infect cells, in the presence of 1 µg/mL polybrene. After two rounds of infection antibiotic treatment was applied as follows: 200 ug/mL Zeocin (Invitrogen) for LZRS vectors and 8 ug/mL of blasticidin for PMX vectors. For CT26 cell transductions, 293T cells were used for virus production: the indicated plasmids were co-transfected and the packaging plasmids pVSVG (Addgene 12260) and HIV (gag-pol). For lentiviral transduction, 293T cells were co-transfected with selected plasmids and 2 µg of pVSVG (Addgene 12260) and 3.72 µg of psPAX2 (Addgene 8454) using Lipofectamine 2000 (Invitrogen). Viral infection and subsequent selection was performed as above. For positive clone selection blasticidin (8 µg/mL) or puromycin (10µg/mL) was used. CRISPR/Cas9 KO cells were generated by lentiviral transduction as described above and positive clones were selected with puromycin (1µg/mL).

Generation of ρ^0 cells

SVEC cells were cultured in the presence of ethidium bromide (EtBr, 500 ng / mL) for a week to generate mitochondrial DNA (mtDNA) depleted cells (ρ^0 cells). Total DNA was extracted and qPCR was performed. The mitochondrial content was measured by the ratio of mtDNA (Dloop) vs genomic DNA (Tert) as measured by

qPCR. Primers: Dloop_FW: AATCTACCATCCTCCGTGAAACC, Dloop_REV: TCAGTTTAGCTACCCCCAAGTTTAA, Tert_FW: CTAGCTCATGTGTCAAGACCCTCTT, Tert_REV: GCCAGCACGTTTCTCTCGTT.

Bone marrow-derived macrophage (BMDM) isolation

Macrophages were generated from bone marrow precursors as described previously [40]. Briefly, bone marrow stem cells were isolated from mice by flushing the bone marrow with PBS. Bone marrow stem cells were differentiated into macrophages by culturing them for 6 days in RPMI medium containing M-CSF (10 ng/mL). Media (containing M-CSF) was replaced after 3 days. Where indicated, BMDM's were isolated from wild-type and *Tnfr1*$^{-/-}$ mice as previously described [41].

qRT-PCR

RNA was isolated from cells using QIAGEN RNeasy Mini Kit (Qiagen) and used for cDNA synthesis and PCR with DyNAmo SYBR Green 2-step qRT-PCR kit (Thermo Fisher Scientific). PCR was performed on a C1000Tm Thermal Cycler (CFX96 Tm-Real time system, BioRad) as following: 3 min at 95 °C, followed by 40 cycles of 20 sec at 95 °C, 30 sec at 57 °C, 30 sec at 72 °C and final 5 min at 72 °C. Relative mRNA quantification was performed by using the 2^-ddCT method for multiple genes. Primer sequences are provided in the supplemental experimental procedures (Supplemental Table 4).

Microscopy

Cells were fixed in 4% PFA/PBS for 10 minutes and then permeabilised with 0.2% Triton/PBS for 10 minutes followed by 1 hour incubation at room temperature with blocking buffer (2% BSA/PBS). Cells were incubated overnight at 4°C with the following antibodies: NFκB-p65 (sc-372, Santa Cruz, 1/300 dilution in blocking buffer),

NFκB-p65 (8242P, Cell Signalling, 1/400 dilution in blocking buffer) and cytochrome *c* (556432, BD Biosciences, 1/300 dilution in blocking buffer). The secondary antibodies used for detection were Alexa Fluor 594 goat anti-rabbit (A11037, Invitrogen, 1/300 dilution), Alexa Fluor 594 goat anti-mouse (A11032, Invitrogen, 1/300 dilution), Alexa Fluor 647 goat anti-mouse (A21236, Invitrogen, 1/300 dilution). DAPI (Vector Lavoratories, H-1200) was used for nuclear staining. Cells undergoing MOMP were scored by the diffusion or loss of cytochrome *c* staining. Cells undergo MOMP were scored as positive with nuclear p65 translocation by co-staining with DAPI. As a positive control of p65 nuclear translocation TNF treatment was used. Data represents the mean of the total number of fields obtained from three independent experiments. Images were taken using a Nikon A1R confocal microscope and analyzed with Image J 1.47i. List of antibodies used is also provided in Supplemental Table 6.

Western blotting

Cells were lysed in NP-40 lysis buffer (1% NP-40, 1mM EDTA, 150mM NaCl, 50mM Tris pH7.4, 1mM PMSF and complete protease inhibitors (Roche)). Protein concentration was determined using the Bradford (BioRad) assay. Proteins were separated by SDS-PAGE and transferred onto nitrocellulose membrane. The membranes were blocked and incubated with one of the following primary antibodies overnight in 4^{o}C: anti-PARP (9532, Cell Signalling, 1/1000), anti-β-Actin (8691001, MP Biomedicals, 1/10000 dilution), anti-α-Tubulin (T5168, Sigma, 1/10000 dilution), anti-Mcl-1 (sc-819, Santa Cruz, 1/1000 dilution), anti-RIPK3 (ADI-905-242-100, Enzo life sciences, 1/1000 dilution), anti-MLKL (ab172868, Abcam, 1/500 dilution), anti-BAK (12105, Cell Signalling, 1/1000 dilution), anti-BAX (Santa Cruz, sc-493, 1/1000 dilution), anti-Caspase-9 (9504P, Cell Signalling, 1/1000 dilution), anti-p-I κBα (2859, Cell Signaling, 1/1000), anti-IκBα (9242, Cell Signaling, 1/1000), anti-NIK (4994P, Cell Signalling, 1/500 dilution), anti-cIAP1 (ALX-803-335-C100, ENZO, 1/1000 dilution), anti-Omi (2176, Cell Signalling, 1/1000 dilution), anti-SMAC (32023, Abcam, 1/1000 dilution), anti-STING (13467S, Cell Signalling, 1/1000 dilution), anti-APAF-1

(8723, Cell Signalling, 1/500 dilution), anti-NFκB-p65 (8242P, Cell Signalling, 1/1000 dilution), anti-p100/p52 (4882, Cell Signalling, 1/500 dilution), anti-NEMO (2685, New England Biolabs, 1/1000), anti-IKKβ (MAB7155, R&D systems, 1/1000), anti-RelB (4954, Cell Signalling, 1/500 dilution), anti-BID (raised against a GST fusion protein of full-length human BID [42]), anti-cleaved caspase-3 (9661, Cell Signaling, 1/1000 dilution), anti-cleaved caspase-7 (9491, Cell Signaling, 1/1000 dilution). Protein detection was achieved with chemoluminescence by the use of HRP-linked secondary antibodies and ECL. Where indicated Image J 1.47i was used for densitometry analysis. List of antibodies used is also provided in Supplemental Table 6.

Cell viability assays

Cell viability was determined either by flow cytometry (FACSCalibur, BD Biosciences, San Jose, CA) or IncuCyte FLR imaging system (Essen Bioscience, Ann Arbor, MI), using the non-cell-permeable nuclear staining procedures: 10 μg/mL Propidium Iodide (PI, P3566, Invitrogen - flow-cytometry) or 30nM SYTOX Green (SG, S7020, Invitrogen - Incucyte), respectively, according to the manufacturer's protocols. The number of SYTOX Green positive cells was normalized to the confluency factor and the percentage of SYTOX Green-positive cells was calculated against a control that achieved 100% cell death. FACS Gating strategy for PI staining is outlined in Supplemental Figure 8.

Flow cytometry

Flow cytometry was used to characterize the profile of immune cells including macrophages, NK and T cells. BMDMs M1/M2 activation status was analysed using FACSCalibur (BD Biosciences, San Jose, CA) with the following antibodies: APC-CD86-clone: GL1 (B185438, Biolegend, 1/200 dilution), and FITC-CD206 (MMR)-clone: C068C2 (141703, Biolegend, 1/200 dilution). Subcutaneous CT26 tumours were isolated from Balb/C mice, homogenised and analyzed for immune cell infiltration

(M1/M2 macrophages, T cells) by BD FACSVerse (BD Biosciences, USA) using the following antibodies: purified anti-mouse CD16/32 / Fc-Block (101302, Biolegend, 1/200 dilution), PerCP/Cy5.5-F4/80- clone BM8 (123128, BD Biosciences, 1/200 dilution), APC-MHC-II/ I-A, I-E, clone: M5/114.15.2 (107614, BD Biosciences, 1/200 dilution), and FITC-CD2O6 (MMR)-clone: C068C2 (141703, Biolegend, 1/200 dilution), Biotin-Hamster CD3e-clone:145-2C11,
(553060, BD-Pharmigen, 1/200 dilution), PE-Streptavidin (405203, Biolegend, 1/2000 dilution). Tumour infiltrated macrophages were further analysed for M1/M2 activation status using the Attune NxT (Thermo Fischer Scientific) flow cytometer with the following antibodies: PerCP/Cy5.5-F4/80-clone:BM8 (123128, BD Biosciences, 1/200 dilution) PECy5-MHC-II/ I-A, I-E- clone: M5/114.15.2
(107612, Biolegend, 1/200 dilution), APCCy7-CD86-clone: GL-1 (105030, Biolegend, 1/200 dilution), APC-NOS2-clone: CXNFT (17-5920-82, eBioscience, 1/200 dilution), Polyclonal Sheep IgG-PE-Arg1 (IC5868P, R&D Systems, 1/200 dilution) and FITC-CD2O6)-clone: C068C2 (MMR) (141703, Biolegend, 1/200 dilution), DAPI (0.5 µg/ml) or Zombie Yellow (423104,Biolegend, 1/500 dilution) were used as cell death dyes to discriminate live/dead cell populations. FACS Gating strategy is outlined in Supplemental Figure 8. List of antibodies used is provided in Supplemental Table 6.

T-cell activation

Freshly isolated tumours were digested with collagenase (1.5 mg/ml) for 30 minutes in 37^{o}C and subsequently homogenised. 2 x 10^{6} isolated cells were treated with 50 ng/ml PMA, 1 µg/ml ionomycin and 1X Brefeldin A in complete RPMI medium and incubated for 6 hours in corning 96-well plate. Cells were collected, stained with Zombie Yellow cell death dye (1/500 dilution) and analysed by flow cytometry (Attune NxT, Thermo Fischer Scientific) with the following antibodies: APC-CD3-clone: 17A2 (100235, Biolegend, 1/200 dilution), PE-CD4, clone: RM4-4 (116006, Biolegend, 1/200 dilution), PECy7-CD8- clone: 53-6.7 (100721, Biolegend, 1/200 dilution), Brilliant Violet 421-IFNγ- clone: XMG1.2 (505829, Biolegend, 1/200 dilution), FITC-

Granzyme B- clone; GB11 (515403, Biolegend, 1/200). FACS Gating strategy is outlined in Supplemental Figure 8. List of antibodies used is also provided in Supplemental Table 6.

ELISA and Luminex assay

Conditioned media was concentrated using the Amicon Ultra-4 Centrifugal Filter Unit with Ultracel-3 membrane (UFC800324, 3 kDa cut-off, Milipore), according to the manufacturer's protocol. TNF protein concentration was measured using the Murine TNF Mini ELISA Development Kit (900-M54, Peprotech), according to the manufacturer's protocol. For the Luminex assay a mouse Cytokine Magnetic 20-Plex Panel (LMC0006M, Invitrogen) was used to measure cytokine levels in mouse serum, and tissue culture supernatant (condensed with the Amicon Ultra-4 Centrifugal Filter Unit), according to the provided protocol.

Luciferase assay

SVEC cells (2 x 10^6 cells in 10cm plate) were transfected with 2 µg of empty vector (PGL3) or NF-κB reporters (reporter 1: PGL3-TNF - TNF promoter binding sites, reporter 2: PGL3-NP3 - NF-κB binding sites). Luciferase activity was measured by Glomax / Veritas Microplate Luminometer, according to the manufacturer's protocol (luciferase assay kit E1500, Promega). Each obtained value was normalized to µg of protein of each individual sample and empty vector.

Immunohistochemistry (IHC)

IHC was performed on 10% buffer-formalin fixed, paraffin-embedded sections (4 µm thick). Staining was performed using a Dako autostainer. Anti-caspase-3, ASP-

175 (9661, Cell Signalling) was used at 1/50 dilution after antigen retrieval with PT buffer (pH 6.0). Anti-CD3 (VP-RM01, Vector Labs) was used at 1/60 dilution after antigen retrieval with PT buffer (pH 6.0). Anti-F4/80 (ab6640, AbCam) was used at 1/400 dilution after antigen retrieval with Proteinase K for 10 minutes.

In silico analysis

Protein correlation analysis as well as survival curves of clinical samples (Kidney renal cell carcinoma), have been generated by using the TCPA (The Cancer Proteome Atlas) bioinformatic-platform provided by MD Anderson Cancer Centre [43].

In vivo experiments

Experiments with Balb/C mice were done in accordance with UK regulations under project license PPL 70/8645, ethical review (University of Glasgow) and the EU Directive 2010. To observe the effect of Apaf1 on tumour growth *in vivo*, 0.5 × 10^6 CT26 GFP tBID 2A BCL-2 (proficient) and CT26 GFP tBID 2 BCL-2 APAF-1^{SH} (deficient) cells were suspended in 200 µl PBS and were subcutaneously implanted into the flank of 6 week old Balb/C female mice (Charles River, UK). Once tumour volumes reached approximate 100 mm^3 (length × $width^2$/2), mice were ranked and randomly divided into four groups. Mice were orally dosed four times over a two-week period with 100 µl Vehicle (10% ethanol, 30% PEG glycol 400, and 60% Phosal 50 PG) or ABT-263 (100mg/kg, diluted in vehicle). Tumours were measured by caliper thrice weekly and mice were killed humanely when tumours reached clinical endpoint of predetermined size or ulceration. Furthermore, mice that were orally dosed two times over a one-week period of time were humanely killed and tumours were assessed for immune cell infiltration either by FACS or by IHC.

For NOD scid gamma $c^{-/-}$ (NSG) experiments, 6 week old NSG mice were

subcutaneously injected with 0.5×10^6 APAF1 KD CT26 cells expressing GFP-tBID 2A Bcl2 cells resuspended in 200 µl of PBS. Once tumor volume reached approximately 100 mm^3 (length x $width^2/2$), mice were given 100 µl of Vehicle (10% Ethanol, 30% PEG glicol 400, and 60% Phosal 50 PG) or ABT-263 (diluted in vehicle) orally four times over a one week period. The animals were then inspected three times a week for tumor development. Once tumors started to develop they were measured every day using a caliper. Mice were humanely killed when tumors reached a predetermined size.

In vivo T-cell depletion

As described previously, CT26 cells expressing eGFP-tBID 2A BCL-2 together with pLKO1-shAPAF-1 (APAF-1^{SH}) were injected subcutaneously into 6 weeks old Balb/C mice ($5x10^5$ cells/mouse). Once tumor volume reached approximately 100 mm^3 Following tumour formation, mice were initially treated with 400 µg of isotype control or anti-Thy.1 (I.P injection) and then were continued to be treated with 200 µg twice per week. Efficiency of T cell depletion was checked by flow cytometric analysis of spleen samples. FACS Gating strategy is outlined in Supplemental Figure 8. List of antibodies used is provided in Supplemental Table 6.

Statistics and Reproducibility

For the *in vitro* experiments, normal distribution was assumed, whereas for the *in vivo* experiments normal distribution has been tested prior the use of the appropriate statistical test. Two-tailed unpaired t-test was used for comparison of two groups, whereas the one-, two-way Analysis of Variance (ANOVA) and non-parametric one-way ANOVA (Kruskal-Wallis) was used for comparison of multiple groups. Spearman's rank test was used for correlation analysis. Cox and Log-Rank p-value were used for survival curve (Kaplan Meier) analyses. Finally, two-tailed Chi-Square was used to determine any significant differences in frequencies of complete tumour regression between two groups. Analyses were performed using Prism 6.0 software (GraphPad).

Data availability

Source data for Figures 2d-e, 2g-i, 3f, 3h, 4d, 5a-d, 5g, 6a, 6c-f and Supplemental Figures S1K, S4a-d, S4g-h, S4j-l, and S5d-l has been provided as Supplemental Table 5. All other data supporting the findings are available from the corresponding author upon reasonable request.

References

37. Lecis, D. *et al.* Dimeric Smac mimetics/IAP inhibitors as in vivo-active pro-apoptotic agents. Part II: Structural and biological characterization. *Bioorg Med Chem* **20**, 6709-6723 (2012).
38. Shalem, O. *et al.* Genome-scale CRISPR-Cas9 knockout screening in human cells. *Science* **343**, 84-87 (2014).
39. Sanjana, N.E., Shalem, O. & Zhang, F. Improved vectors and genome-wide libraries for CRISPR screening. *Nat Methods* **11**, 783-784 (2014).
40. Graczyk, D., White, R.J. & Ryan, K.M. Involvement of RNA Polymerase III in Immune Responses. *Mol Cell Biol* **35**, 1848-1859 (2015).
41. Peltzer, N. *et al.* HOIP deficiency causes embryonic lethality by aberrant TNFR1-mediated endothelial cell death. *Cell Rep* **9**, 153-165 (2014).
42. Werner, A.B., de Vries, E., Tait, S.W., Bontjer, I. & Borst, J. Bcl-2 family member Bfl-1/A1 sequesters truncated bid to inhibit is collaboration with pro-apoptotic Bak or Bax. *J Biol Chem* **277**, 22781-22788 (2002).
43. Li, J. *et al.* TCPA: a resource for cancer functional proteomics data. *Nat Methods* **10**, 1046-1047 (2013).

Type of file: figure
Label: 1
Filename: figure_1.pdf

Figure 1

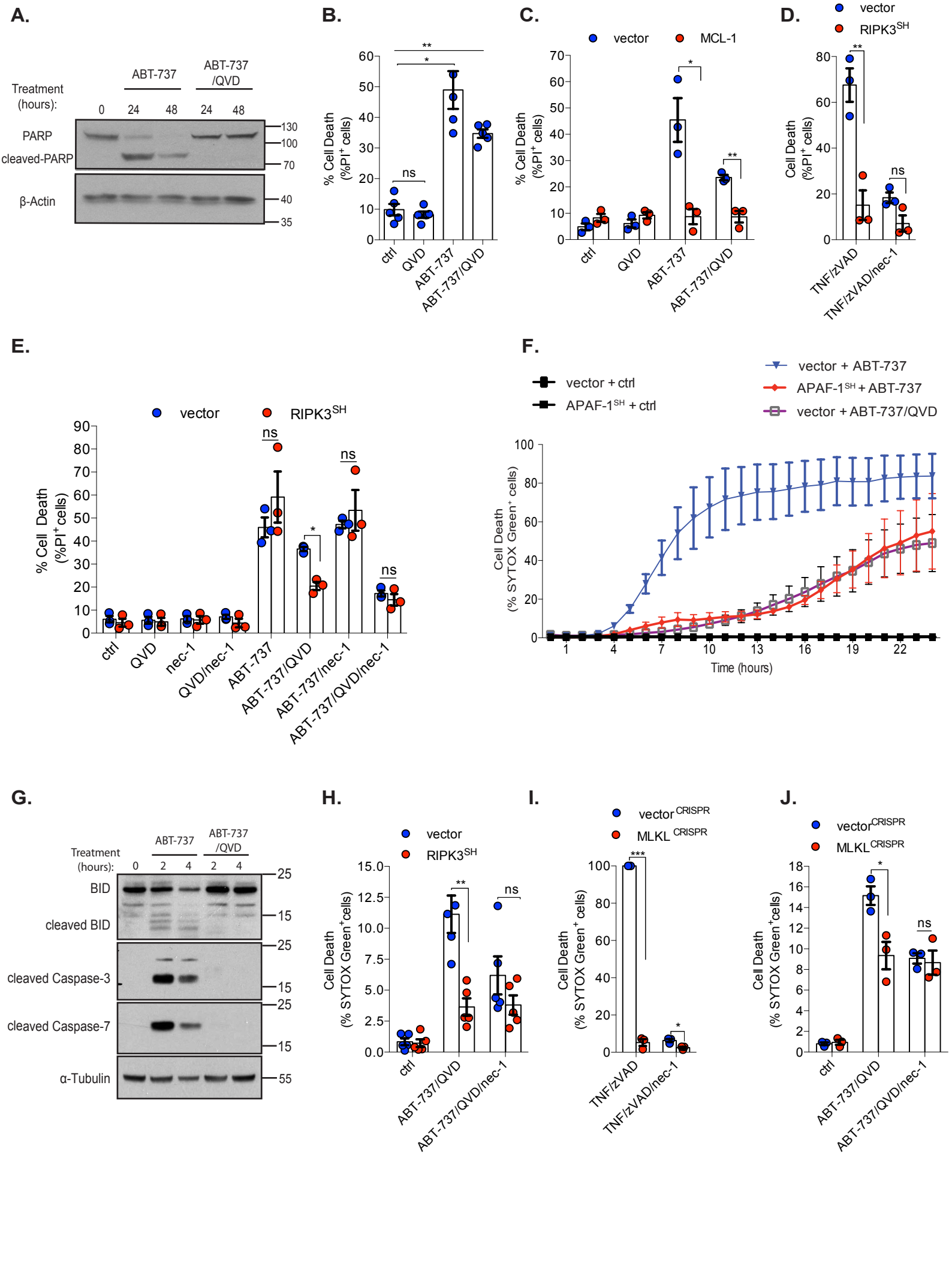
A.
Treatment (hours):
ABT-737
ABT-737 /QVD
0 24 48 24 48
PARP
cleaved-PARP
β-Actin
130
100
70
40
35
B.
% Cell Death (%PI+ cells)
ns
ctrl
QVD
ABT-737
ABT-737/QVD
C.
vector
MCL-1
% Cell Death (%PI+ cells)
ctrl
QVD
ABT-737
ABT-737/QVD
D.
vector
RIPK3SH
Cell Death (%PI+ cells)
TNF/zVAD
TNF/zVAD/nec-1
E.
vector
RIPK3SH
% Cell Death (%PI+ cells)
ctrl
QVD
nec-1
QVD/nec-1
ABT-737
ABT-737/QVD
ABT-737/nec-1
ABT-737/QVD/nec-1
F.
vector + ctrl
APAF-1SH + ctrl
vector + ABT-737
APAF-1SH + ABT-737
vector + ABT-737/QVD
Cell Death (% SYTOX Green+ cells)
Time (hours)
G.
Treatment (hours):
ABT-737
ABT-737 /QVD
0 2 4 2 4
BID
cleaved BID
cleaved Caspase-3
cleaved Caspase-7
α-Tubulin
25
15
25
15
25
15
55
H.
vector
RIPK3SH
Cell Death (% SYTOX Green+ cells)
ctrl
ABT-737/QVD
ABT-737/QVD/nec-1
I.
vectorCRISPR
MLKLCRISPR
Cell Death (% SYTOX Green+ cells)
TNF/zVAD
TNF/zVAD/nec-1
J.
vectorCRISPR
MLKLCRISPR
Cell Death (% SYTOX Green+ cells)
ctrl
ABT-737/QVD
ABT-737/QVD/nec-1

Type of file: figure
Label: 2
Filename: figure_2.pdf

Figure 2

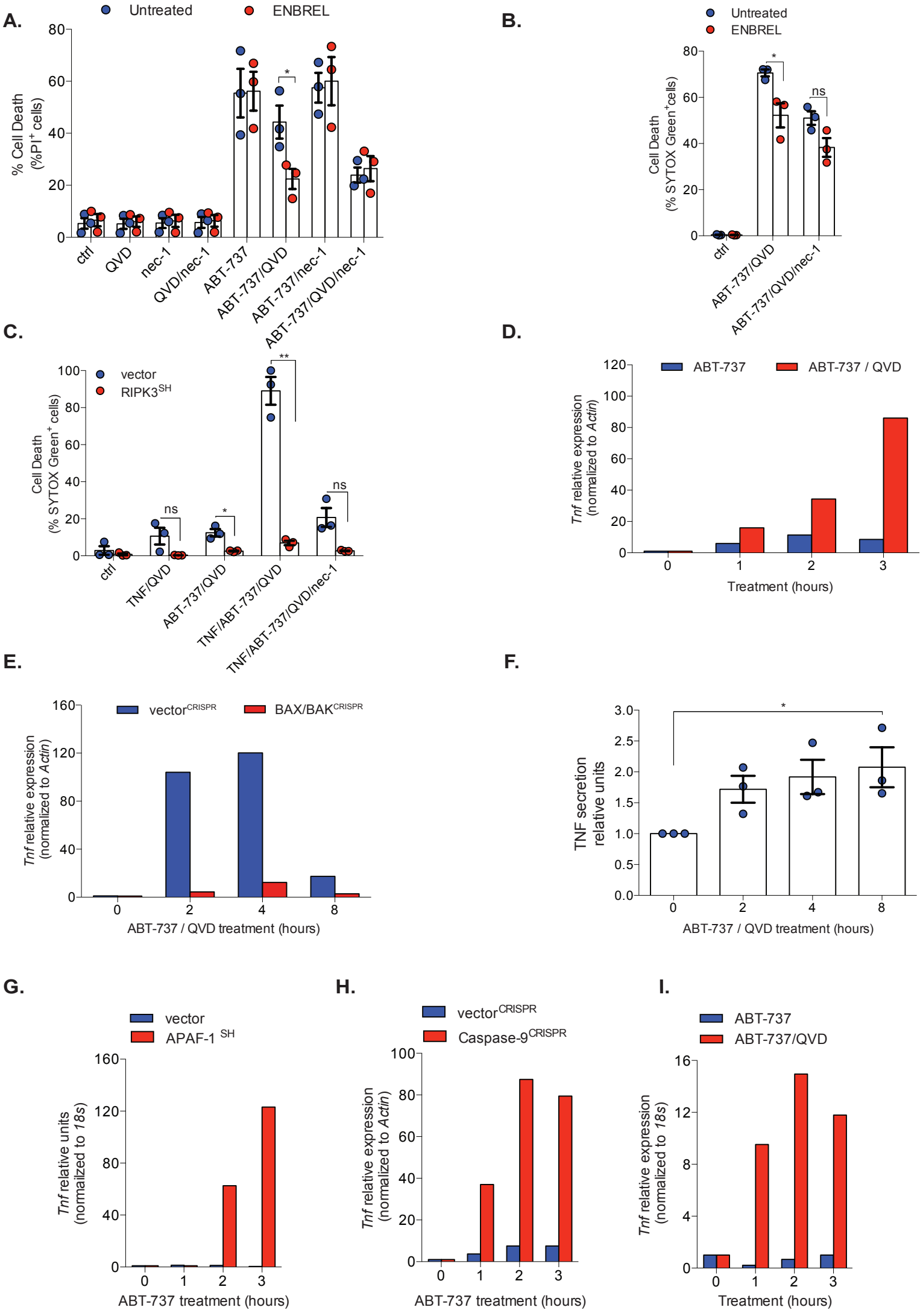
A.
Untreated
ENBREL
% Cell Death (%PI+ cells)
ctrl
QVD
nec-1
QVD/nec-1
ABT-737
ABT-737/QVD
ABT-737/nec-1
ABT-737/QVD/nec-1
B.
Cell Death (% SYTOX Green+cells)
ns
C.
vector
RIPK3SH
TNF/QVD
ABT-737/QVD
TNF/ABT-737/QVD
TNF/ABT-737/QVD/nec-1
D.
ABT-737
ABT-737 / QVD
Tnf relative expression (normalized to Actin)
Treatment (hours)
E.
vectorCRISPR
BAX/BAKCRISPR
ABT-737 / QVD treatment (hours)
F.
TNF secretion relative units
G.
APAF-1 SH
Tnf relative units (normalized to 18s)
ABT-737 treatment (hours)
H.
Caspase-9CRISPR
I.
ABT-737/QVD

Type of file: figure
Label: 3
Filename: figure_3.pdf

Figure 3

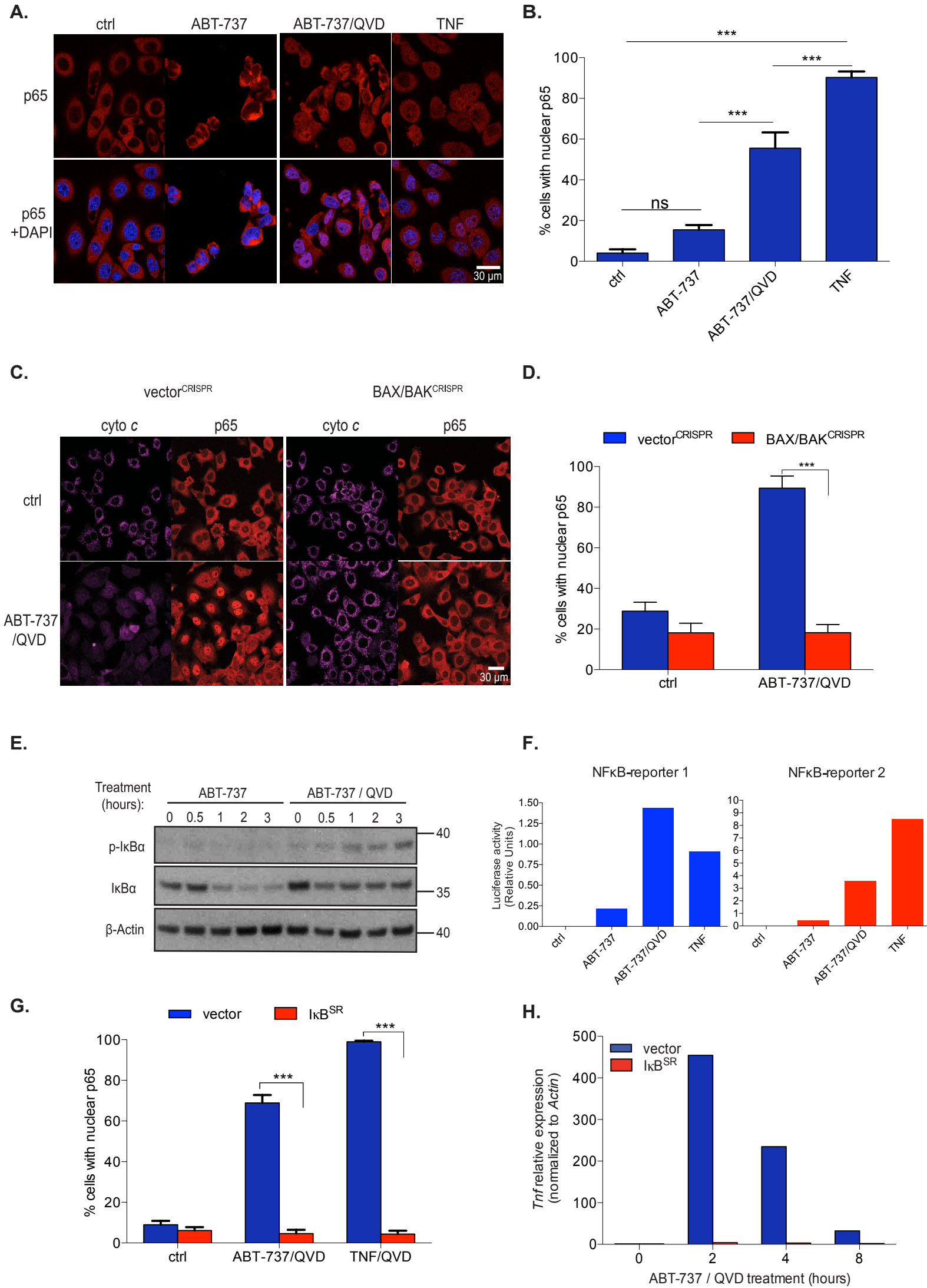
A.
ctrl
ABT-737
ABT-737/QVD
TNF
p65
p65 +DAPI
30 µm
B.
% cells with nuclear p65
ns
***
ctrl
ABT-737
ABT-737/QVD
TNF
C.
vector^CRISPR
BAX/BAK^CRISPR
cyto c
p65
ctrl
ABT-737 /QVD
30 µm
D.
vector^CRISPR
BAX/BAK^CRISPR
% cells with nuclear p65
ctrl
ABT-737/QVD
E.
Treatment (hours):
ABT-737
ABT-737 / QVD
0 0.5 1 2 3 0 0.5 1 2 3
p-IκBα
IκBα
β-Actin
40
35
40
F.
NFκB-reporter 1
NFκB-reporter 2
Luciferase activity (Relative Units)
ctrl
ABT-737
ABT-737/QVD
TNF
G.
vector
IκB^SR
% cells with nuclear p65
ctrl
ABT-737/QVD
TNF/QVD
H.
vector
IκB^SR
Tnf relative expression (nomalized to Actin)
ABT-737 / QVD treatment (hours)

Type of file: figure
Label: 4
Filename: figure_4.pdf

Figure 4

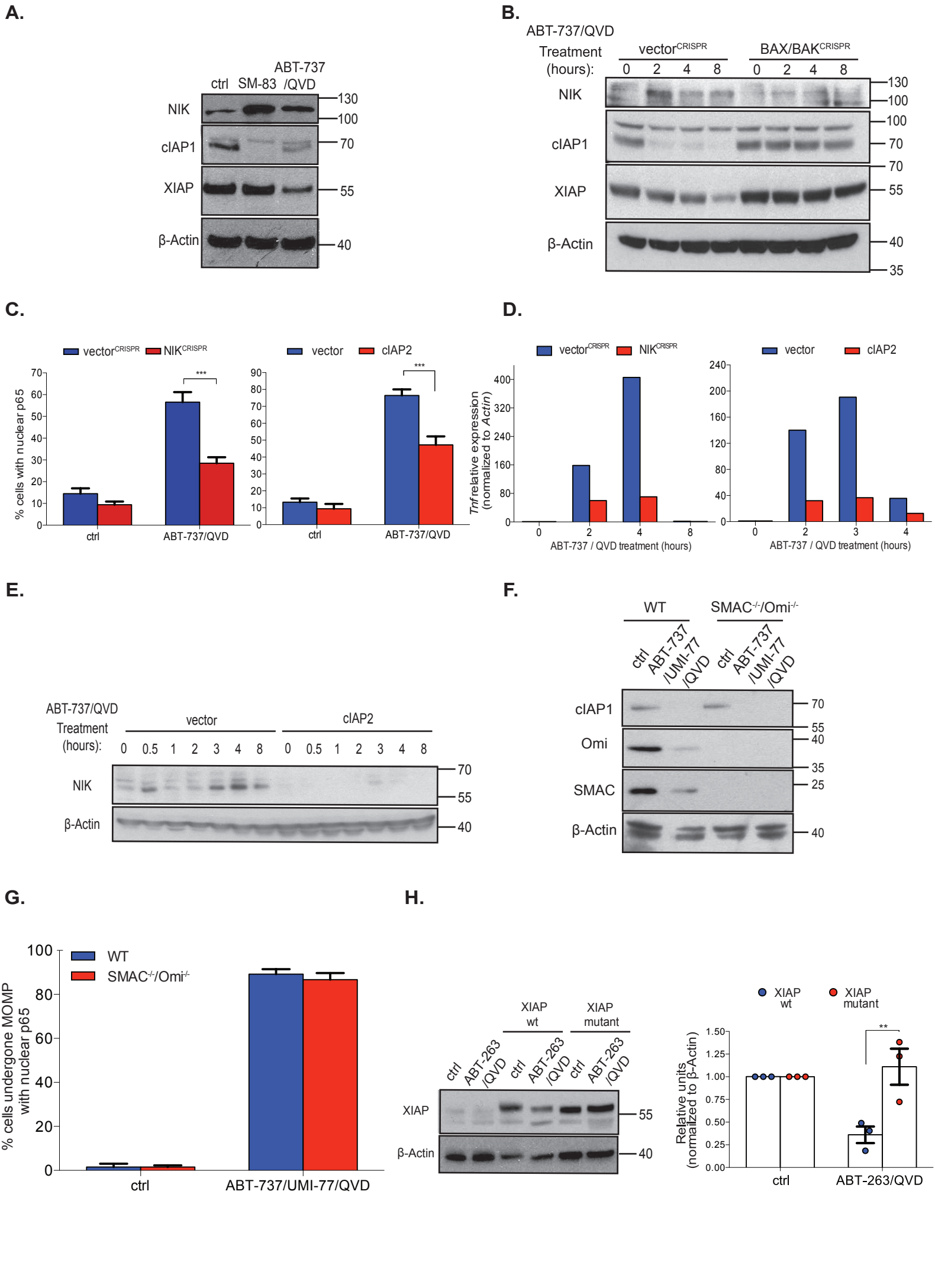
A.
ctrl
SM-83
ABT-737 /QVD
NIK
cIAP1
XIAP
β-Actin
130
100
70
55
40
B.
ABT-737/QVD
Treatment (hours):
vector^CRISPR
BAX/BAK^CRISPR
0 2 4 8 0 2 4 8
NIK
cIAP1
XIAP
β-Actin
130
100
100
70
70
55
40
35
C.
vector^CRISPR
NIK^CRISPR
vector
cIAP2
% cells with nuclear p65
***
ctrl
ABT-737/QVD
D.
vector^CRISPR
NIK^CRISPR
vector
cIAP2
Tnf relative expression (normalized to Actin)
ABT-737 / QVD treatment (hours)
E.
ABT-737/QVD
Treatment (hours):
vector
cIAP2
0 0.5 1 2 3 4 8 0 0.5 1 2 3 4 8
NIK
β-Actin
70
55
40
F.
WT
SMAC-/-/Omi-/-
ctrl
ABT-737 /UMI-77 /QVD
cIAP1
Omi
SMAC
β-Actin
70
55
40
35
25
40
G.
WT
SMAC-/-/Omi-/-
% cells undergone MOMP with nuclear p65
ctrl
ABT-737/UMI-77/QVD
H.
XIAP wt
XIAP mutant
ctrl
ABT-263 /QVD
XIAP
β-Actin
55
40
XIAP wt
XIAP mutant
Relative units (normalized to β-Actin)
**
ctrl
ABT-263/QVD

Type of file: figure
Label: 5
Filename: figure_5.pdf

Figure 5

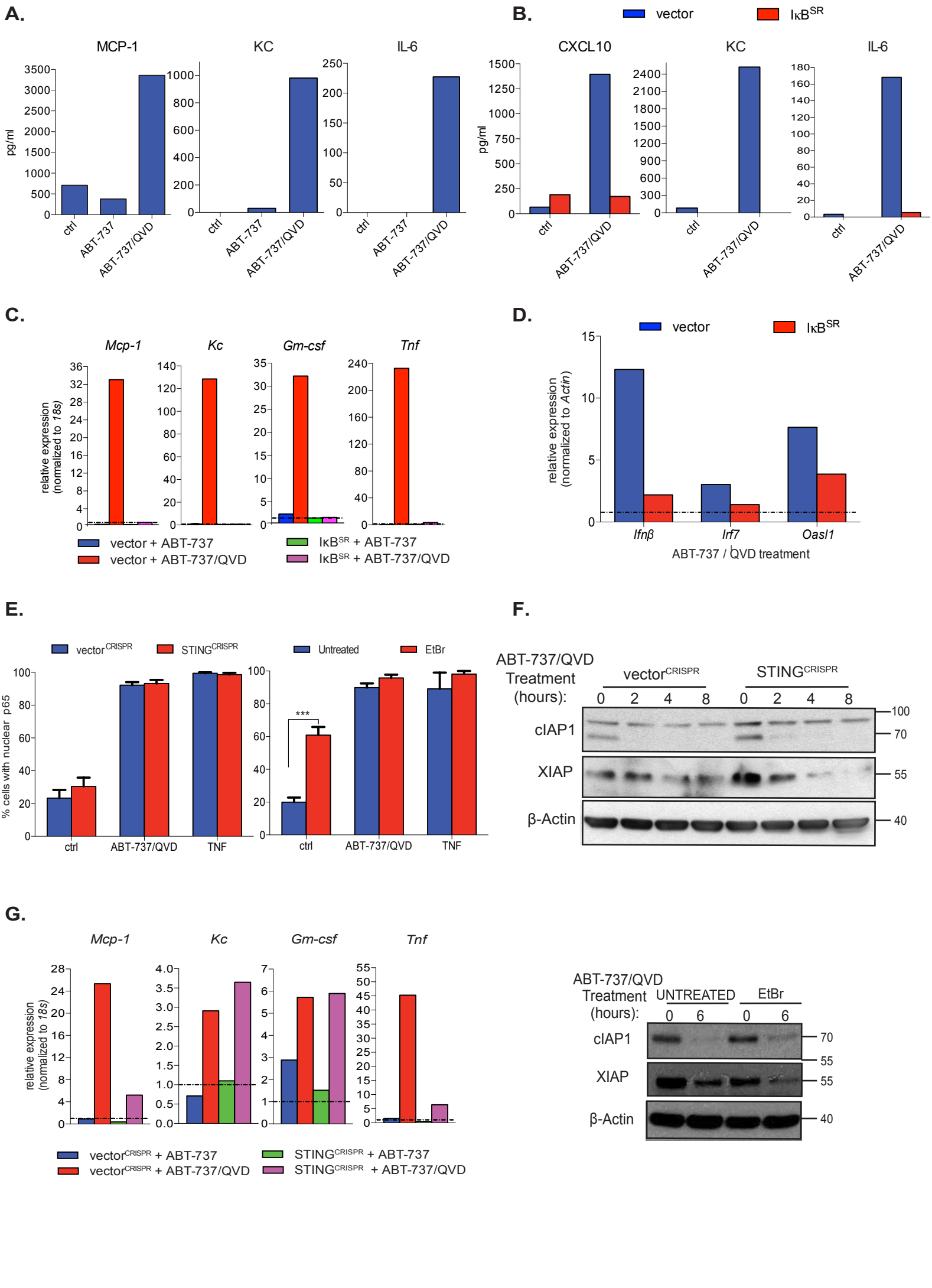
A.
MCP-1
KC
IL-6
pg/ml
ctrl
ABT-737
ABT-737/QVD
B.
vector
IκB^SR
CXCL10
KC
IL-6
C.
Mcp-1
Kc
Gm-csf
Tnf
relative expression (normalized to 18s)
vector + ABT-737
vector + ABT-737/QVD
IκB^SR + ABT-737
IκB^SR + ABT-737/QVD
D.
relative expression (normalized to Actin)
Ifnβ
Irf7
Oasl1
ABT-737 / QVD treatment
E.
vector^CRISPR
STING^CRISPR
Untreated
EtBr
% cells with nuclear p65
***
ctrl
ABT-737/QVD
TNF
F.
ABT-737/QVD Treatment (hours):
vector^CRISPR
STING^CRISPR
0 2 4 8 0 2 4 8
cIAP1
XIAP
β-Actin
100
70
55
40
G.
Mcp-1
Kc
Gm-csf
Tnf
relative expression (normalized to 18s)
vector^CRISPR + ABT-737
vector^CRISPR + ABT-737/QVD
STING^CRISPR + ABT-737
STING^CRISPR + ABT-737/QVD
ABT-737/QVD Treatment (hours):
UNTREATED
EtBr
0 6 0 6
cIAP1
XIAP
β-Actin
70
55
55
40

Type of file: figure
Label: 6
Filename: figure_6.pdf

Figure 6

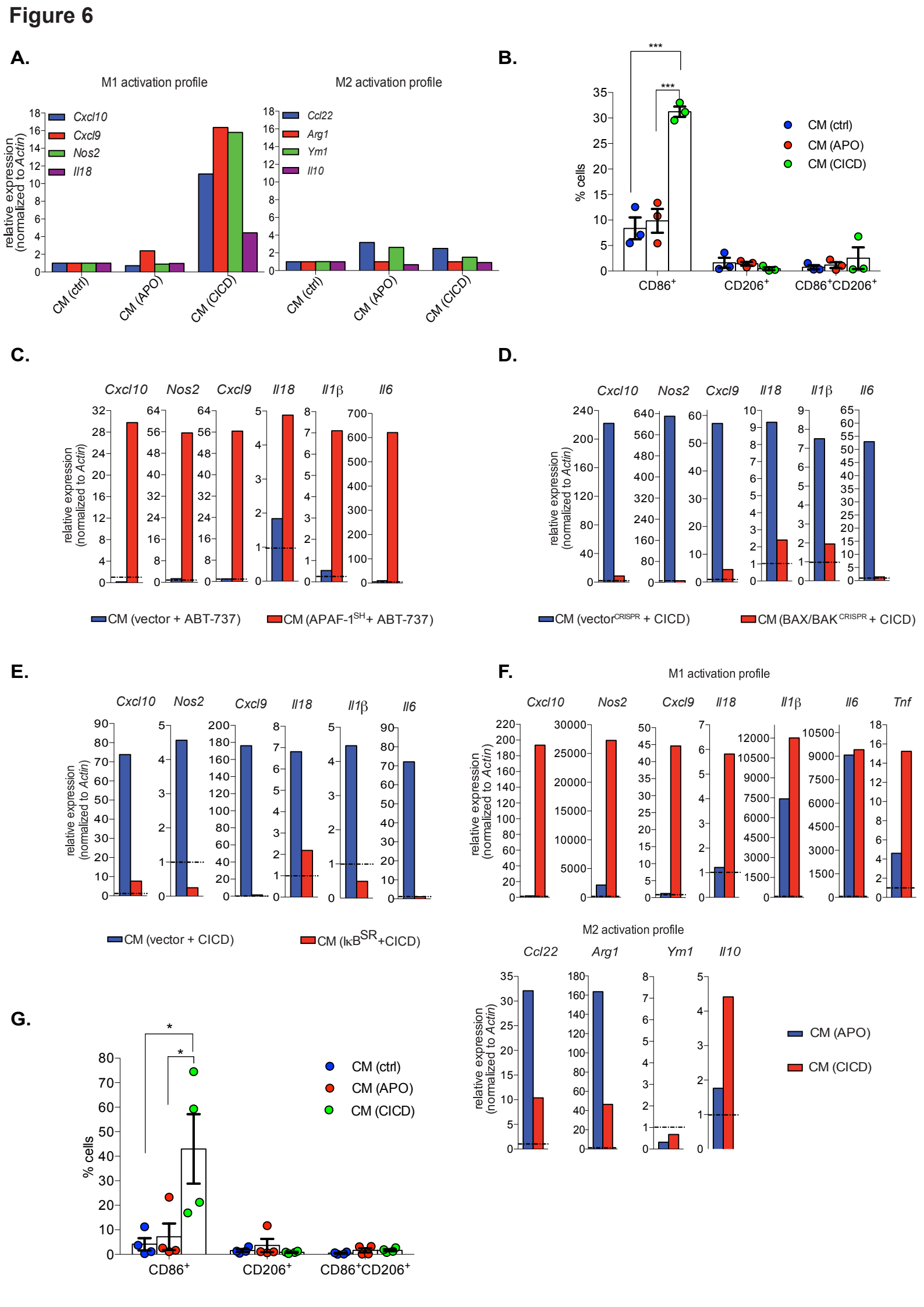
A.
M1 activation profile
M2 activation profile
relative expression (normalized to Actin)
Cxcl10
Cxcl9
Nos2
Il18
Ccl22
Arg1
Ym1
Il10
CM (ctrl)
CM (APO)
CM (CICD)
B.
% cells
CM (ctrl)
CM (APO)
CM (CICD)
CD86+
CD206+
CD86+CD206+
C.
Cxcl10
Nos2
Cxcl9
Il18
Il1β
Il6
relative expression (normalized to Actin)
CM (vector + ABT-737)
CM (APAF-1SH+ ABT-737)
D.
CM (vectorCRISPR + CICD)
CM (BAX/BAKCRISPR + CICD)
E.
CM (vector + CICD)
CM (IκBSR+CICD)
F.
M1 activation profile
Tnf
M2 activation profile
G.

Type of file: figure
Label: 7
Filename: figure_7.pdf

Figure 7

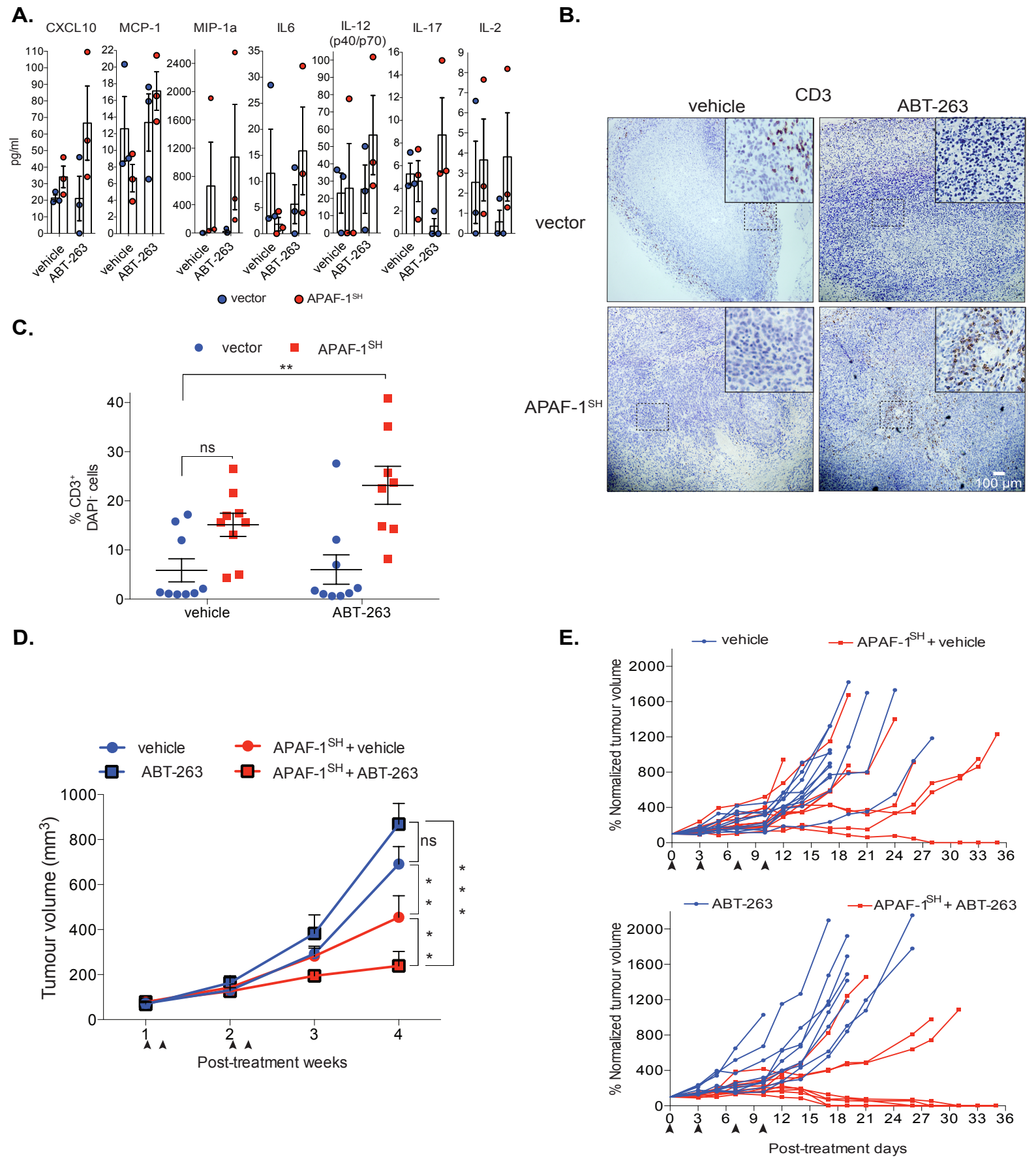
A.
CXCL10
MCP-1
MIP-1a
IL6
IL-12 (p40/p70)
IL-17
IL-2
pg/ml
vehicle
ABT-263
vector
APAF-1SH
B.
CD3
vehicle
ABT-263
vector
APAF-1SH
100 µm
C.
vector
APAF-1SH
**
ns
% CD3+ DAPI- cells
vehicle
ABT-263
D.
vehicle
ABT-263
APAF-1SH + vehicle
APAF-1SH + ABT-263
Tumour volume (mm3)
ns
Post-treatment weeks
E.
vehicle
APAF-1SH + vehicle
% Nomalized tumour volume
ABT-263
APAF-1SH + ABT-263
Post-treatment days

Type of file: figure
Label: 8
Filename: figure_8.pdf

Figure 8

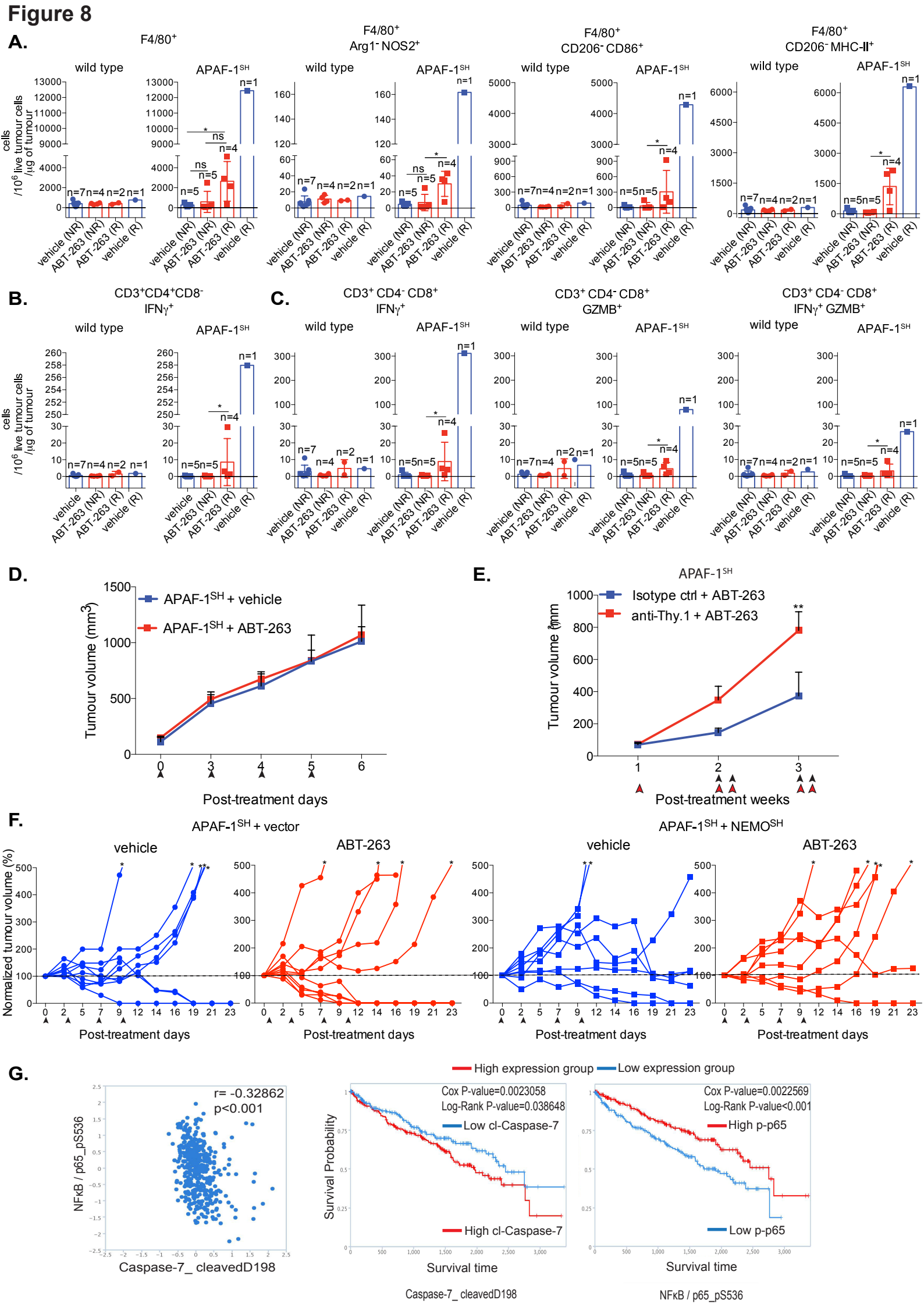
A.
F4/80+
F4/80+ Arg1- NOS2+
F4/80+ CD206- CD86+
F4/80+ CD206- MHC-II+
wild type
APAF-1SH
cells /10^6 live tumour cells /µg of tumour
vehicle (NR)
ABT-263 (NR)
ABT-263 (R)
vehicle (R)
B.
CD3+CD4+CD8- IFNγ+
C.
CD3+ CD4- CD8+ IFNγ+
CD3+ CD4- CD8+ GZMB+
CD3+ CD4- CD8+ IFNγ+ GZMB+
D.
APAF-1SH + vehicle
APAF-1SH + ABT-263
Tumour volume (mm3)
Post-treatment days
E.
APAF-1SH
Isotype ctrl + ABT-263
anti-Thy.1 + ABT-263
Tumour volume (mm3)
Post-treatment weeks
F.
APAF-1SH + vector
APAF-1SH + NEMOSH
vehicle
ABT-263
Nomalized tumour volume (%)
Post-treatment days
G.
r= -0.32862
p<0.001
NFκB / p65_pS536
Caspase-7_ cleavedD198
High expression group
Low expression group
Cox P-value=0.0023058
Log-Rank P-value=0.038648
Low cl-Caspase-7
High cl-Caspase-7
Survival Probability
Survival time
Cox P-value=0.0022569
Log-Rank P-value<0.001
High p-p65
Low p-p65

Europe PMC plus has received the file 'supp_info_1.docx' as supplementary data. The file will not appear in this PDF Receipt, but it will be linked to the web version of your manuscript.

Europe PMC plus has received the file 'supp_info_10.pdf' as supplementary data. The file will not appear in this PDF Receipt, but it will be linked to the web version of your manuscript.

Europe PMC plus has received the file 'supp_info_2.pdf' as supplementary data. The file will not appear in this PDF Receipt, but it will be linked to the web version of your manuscript.

Europe PMC plus has received the file 'supp_info_3.pdf' as supplementary data. The file will not appear in this PDF Receipt, but it will be linked to the web version of your manuscript.

Europe PMC plus has received the file 'supp_info_4.pdf' as supplementary data. The file will not appear in this PDF Receipt, but it will be linked to the web version of your manuscript.

Europe PMC plus has received the file 'supp_info_5.pdf' as supplementary data. The file will not appear in this PDF Receipt, but it will be linked to the web version of your manuscript.

Europe PMC plus has received the file 'supp_info_6.pdf' as supplementary data. The file will not appear in this PDF Receipt, but it will be linked to the web version of your manuscript.

Europe PMC plus has received the file 'supp_info_7.pdf' as supplementary data. The file will not appear in this PDF Receipt, but it will be linked to the web version of your manuscript.

Europe PMC plus has received the file 'supp_info_8.pdf' as supplementary data. The file will not appear in this PDF Receipt, but it will be linked to the web version of your manuscript.

Europe PMC plus has received the file 'supp_info_9.pdf' as supplementary data. The file will not appear in this PDF Receipt, but it will be linked to the web version of your manuscript.